European Commission

JRC TECHNICAL REPORTS

Electrical Blast simulator (e-BLAST): design, development and first operational tests

Peroni Marco
Solomos George
Pegon Pierre
Caverzan Alessio

2015

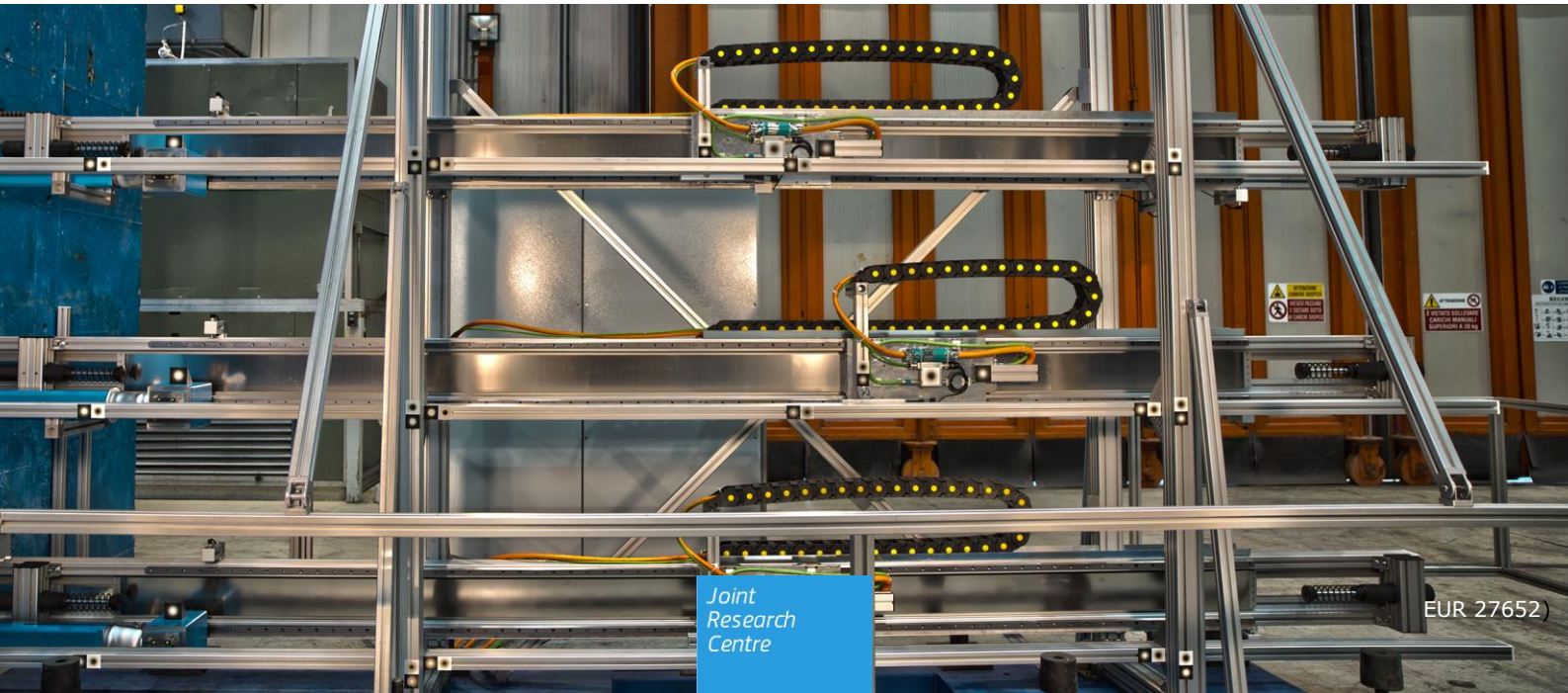

Joint Research Centre

EUR 27652

JRC Science Hub
https://ec.europa.eu/jrc

JRC99592

EUR 27652

ISBN 978-92-79-54184-1

ISSN 1831-9424

doi:10.2788/292788

How to cite: Authors; title; EUR; doi

Electrical Blast simulator (e-BLAST): design, development and first operational tests

Table of contents

Abstract

The Electrical Blast Simulator (e-BLAST) activity involves the development of an apparatus capable of reproducing the effects of a blast pressure wave on large-scale structural components (such as columns, walls, etc.) with the objective of improving their strength in such severe loading situations. The work relates to the BUILT-CIP project which deals with the protection and resilience of the built environment (critical buildings, transportation and energy infrastructure etc.) under catastrophic events such as blast and impacts.

The e-BLAST facility has been conceived and designed with the expertise acquired in the previous project "Blast Simulation Technology Development", supported through an Administrative Arrangement by DG HOME. Differently from the prototype developed in that project, the e-BLAST exploits a recent technology that appears to be very promising in this particular research field. Specifically, three synchronous electrical linear motors have been adopted for accelerating the impacting masses. This choice has led to develop a more effective, versatile and low-cost facility.

The report presents in detail the facility design, its components and their assembly, and a series of preliminary tests carried out in the ELSA laboratory in order to assess the performance of the e-BLAST. Finally, a brief description of further developments and feasible large-scale structural tests, planned to be performed with the new facility, are discussed.

1. Introduction

Critical infrastructures in fields such as energy, health, communication, government, transport etc. are made of physical structures, or are housed in physical structures. Such structures may naturally become the target of terrorist bombing attacks. Measures to protect them (involving prevention, intelligence, detection, deterrence etc.) will certainly be taken, but if everything fails, it is very important that the mechanical structure itself mitigates some effects of the explosion and maintains certain functionalities.

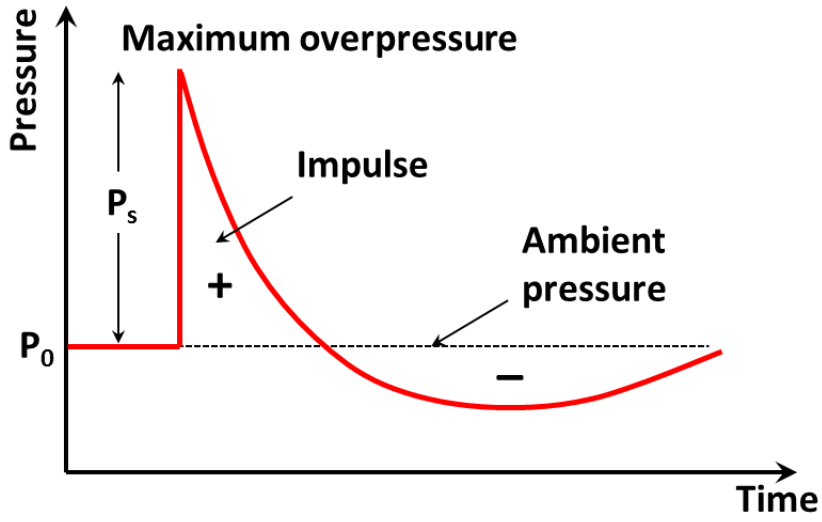

Figure 1. Blast wave pressure characteristic in free-air explosions

A typical pressure wave curve (which eventually will load a structure) at some distance from an explosion is shown in Figure 1. Its main characteristics concerning damaging effects on structures are the magnitude of the overpressure, the duration of the positive phase and especially its impulse, i.e., the area under the curve over the positive phase. This impulsive load will be delivered to a structure in a few milliseconds forcing it to respond or fail in a peculiar mode. This necessitates that models and design techniques for blast resistant structures be thoroughly validated with reliable data from field tests. However, such tests with actual explosions are expensive and they are usually performed within military grounds. Thus, alternative testing methods are desirable, and this has been the case at the University of California in San Diego, where the first blast simulator facility was built in 2006. As claimed, the effects of bombs are generated without the use of explosive materials. The facility produces repeatable, controlled blast load simulations on full-scale columns and other structural components. The simulator recreates the speed and force of explosive shock waves through servo-controlled hydraulic actuators that punch properly the test specimens.

With the ongoing work, a similar blast simulation capability has been developed within the EU by the JRC. The staff of the ELSA Unit has a long and strong experience in the servo-controlled actuators. In fact, some of these devices have been constructed in-house and relevant technology has been transferred to other European laboratories. Concerning the currently required fast actuators, an alternative design concept has been implemented [1] and tested [2-3], which is capable of generating impact loads resembling closely those of the real explosions of Figure 1. This last feature has been also thoroughly investigated via advanced numerical simulations in order to ensure the possibility of reproducing blast loads using suitable impacting masses [4-5]. The fast actuator, as designed in [1], is a mixed pneumatic/mechanical equipment. Dubbed for short "g-BLAST", it is based on a mechanical spring and pressurised nitrogen gas

propulsion that can accelerate masses of about 50 kg to a maximum velocity of about 20 m/s. This has allowed the realistic testing of components to "simulated" explosions and has provided the necessary data for the verification and validation of numerical simulation tools. This activity was conducted in the project "Blast Simulation Technology Development", supported through the Administrative Arrangement No JRC 32253-2011 by DG HOME.

However, during the g-BLAST prototype testing a series of shortcomings has been experienced for which new technological solutions have been considered. The main drawbacks of the pneumatic/mechanical actuator include:

- Large "inactive" masses. The g-BLAST has a mass of 1.5 tons and the mechanical-damper support for one actuator reaches about 3 tons. It is obvious that these huge "inactive" masses, compared with the accelerated mass (of about 50 kg), create a problem, especially if several actuators must be simultaneously placed. In fact, the support must be stiff enough to resist the strong reaction force that the actuator generates during the operation.
- Synchronization problems. The only effective solution to synchronize more than one g-BLAST actuators to operate simultaneously is to adopt a mechanical fragile bolt, the fracture of which would be triggered by detonating a small explosive charge. This fact is in contrast with the main objective of avoiding any use of explosives during the experiments. In addition, also in the case of such a synchronized start of the different actuators (triggered by an explosive charge), there would be no certainty that the impacting masses would arrive to the tested specimen at the same instant.
- Test execution complexity. The operation of the g-BLAST involves different sub-actuators (the hydraulic jack for the pre-stressing of the mechanical spring and the booster for the pressurized nitrogen) that make the execution of a g-BLAST test quite complex and lengthy. In addition, the release of the shaft (with the attached impacting mass) starts when a critical stress is reached in the fragile bolt and this value varies, depending on the fragile material properties. For this reason, it is impossible to foresee with precision some test parameters, such as the starting time or the final impact-mass velocity.

Different from the prototype developed in the previous project, the new e-BLAST facility exploits a recent technology that seems to be very promising in this particular research field. In principle, the fast actuator for the acceleration of the impacting mass has been replaced by a linear electric motor. Thus three synchronous electrical, linear motors have been adopted to design a more effective, versatile and low-cost facility. The clear advantages of the new technology employed will be discussed in the next paragraphs considering all aspects related to the design, assembly and operation of the facility. Particular attention will be paid to safety procedures and countermeasures due to the intrinsic dangerousness of this type of facility. Finally, a series of preliminary tests carried out in the ELSA laboratory in order to assess the performance of the new e-BLAST will be analysed and discussed and further improvements and testing capabilities will be presented.

It is useful to remind that the development of this technology will be important for both the research and the practicing engineers and architects who need design rules and guidelines. Besides characterizing blast effects on structural systems, the methodology will contribute to evaluating technologies for hardening and retrofitting buildings and bridges against terrorist bomb attacks. Further, it will help in the investigation of the problem of progressive collapse, i.e., the phenomenon where a local failure propagates in a disproportionate manner to lead to global failure, like the building collapse in the Oklahoma City bombing.

It is also appropriate to underline that the whole design of e-BLAST falls entirely within a new application field for the linear motor technology that exploits the maximum performance of the several components involved (the motors themselves, the guiding system and the feedback sensors), as will be discussed below. For these reasons, in order to develop safely the apparatus a meticulous and systematic experimentation procedure has been implemented, essential for reaching satisfactory results.

2. Operation principle and design

As stated before, the e-BLAST exploits a relatively new technology in the research and testing field, based on a particular class of electro-magnetic actuators: the electrical synchronous linear motors.
The linear motor has really come of age in the past decade through a dramatic increase in practical and beneficial industrial applications. The linear motor is often described simply as a rotary motor that has been rolled out flat (figure 2a), and the principles of operation are the same. The forcer (rotor) is made up of coils of wires encapsulated in epoxy, and the track is constructed by placing magnets (usually high power "rare earth" magnets) on steel (figure 2b).

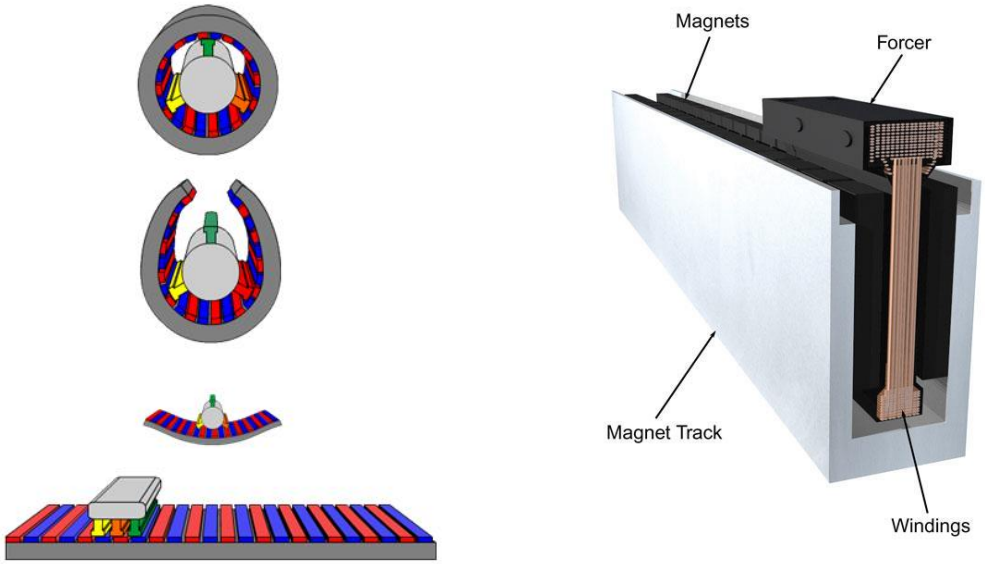

Figure 2. (**a**) Sketch of synchronous electrical linear motor and (**b**) typical industrial assembly

The forcer of the motor contains the windings, Hall-effect board, thermistor (to monitor temperature) and the electrical connections. In rotary motors, the rotor and stator require rotary bearings to support the rotor and maintain the air gap between the moving parts. In the same way, linear motors require linear guide rails to maintain the position of the forcer in the magnetic field of the magnet track. Just as rotary servomotors have encoders mounted to them to give positional feedback of the shaft, linear motors require positional feedback in the linear direction. By using a linear encoder, position is directly measured at the load for increased accuracy of the load position.
The control for linear motors is identical to rotary motors. Like a brushless rotary motor, the forcer and track have no mechanical connection (no brushes). Unlike rotary motors, where the rotor spins and the stator is held fixed, a linear motor system can have either the forcer or the magnet track move (most positioning system applications use a moving forcer and static track). With a moving forcer motor, the forcer weight is small compared with load. However, a cable management system with high-flex cable is required. With a moving track arrangement, the motor must move the load plus the mass of the magnet track, but no cable management system is required.
Similar electromechanical principles apply whether the motor is rotary or linear. The same electromagnetic force that creates torque in a rotary motor creates a force in its linear counterpart. Hence, the linear motor uses the same controls and programmable positioning as a rotary motor.

In the next paragraphs each component of the e-BLAST facility will be presented as well as its design motivation. As a general remark, it can be stated that the whole facility

design is based on the concept of modular design. In this sense, the facility is composed of a series of single standard modules that must be arranged and assembled to reach an optimal solution. This is particularly important in dynamic tests where normally the testing facility must be adapted to the specimen to reach best results.

2.1 Axis module

The core component of the e-BLAST facility is the so called "axis module" that include all sub-components essential to accelerate the impacting masses. This part is mainly composed of three elements: the linear motor, a low-friction railway system and a structural support frame.
After an in-depth market search, it was concluded that the manufacturer able to produce a commercial linear motor with most features comparable with the minimum requirements based on the g-BLAST project was Siemens. Specifically the linear motor selected for the e-BLAST design was the Siemens 1FN3 in the version explicitly developed for peak loads (Figure 3a).

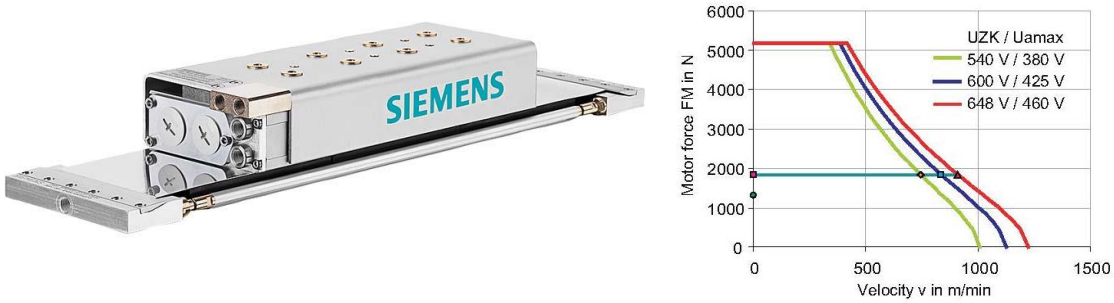

Figure 3. (**a**) Siemens 1FN3 synchronous linear motor and (**B**) motor force–velocity characteristic of selected motor.

The linear motor is essentially composed by a primary section, that is the part connected to the power supply and a secondary section composed by a series of passive high-intensity magnets. For the particular impulsive application, no additional cooling system has been adopted beacuse the active cycle time is substantially lower than the inactivity time and overheating problems are improbable. Figure 3b reports the motor force-velocity characteristic of selected motor that is the main feature for an acceletator facility (the whole datasheet is reported in annex A).

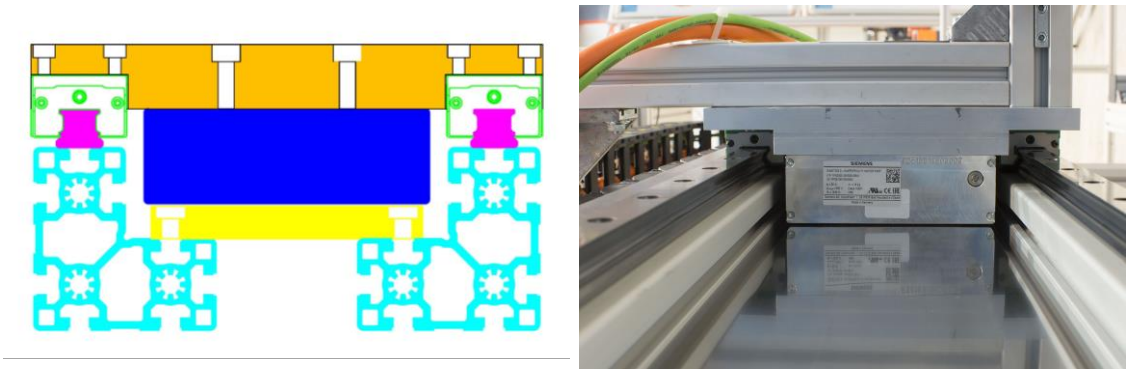

Figure 4. (**a**) Diagram of the section of the set motor + railway + support frame and (**B**) detail of actual axis modulus of e-BLAST.

Considering the motor characteristic and with the suitable acceleration stroke, the 1FN3 motor can accelerate a mass at a maximum velocity of about 16 m/s (1000 m/min with 3 phases power supply) that is totally compatible with di previous g-BLAST facility. As it can be easily noticed, linear motors have a flat characteristic (maximum pushing force) until a certain velocity and after that the force available descreases (increasing the motor velocity) until zero at the so called "electrical stall".
As reported in the motor datasheet, during its operation the attraction force between primary and secondary section reach a value of 10.3 kN. This feature makes essential a suitable sliding system to ensure the operational gap between the two motor sections (that has a tollerance of about tenths of mm) and limit friction forces due to this normal action. The solution adopted consists of a double linear bearing railway that ensure a high stiffness support (to keep constant the operational primary/secondary motor gap) with low friction due to the bearing technology. The linear bearings actually adopted are manufactured by INA and the data sheet is reported in annex B.
The structural support frame has been assembled using a series of aluminium structural elements manufactured by Bosch-Rexroth and the diagram of the section of the set motor + railway + frame is reported in figure 4a. Figure 4b reports otherwise a detail of the actual solution adopted. In the sketch the primary motor section is in blue, the secondary section in yellow, the aluminium frame in cyan, the raylway in magenta and the carriages in green. The orange motor plate connects the four carriages, that slide on the two railways, and has been manufactured with high strength alumium alloy to limit the weight (and consequently inertia phenomena) maintening a suitable stiffness. In order to protect the secondary magnets from metallic dust or unwanted contact between the two motor sections, a stainless steel sheet covers them (Figure 4b).
The axis module, as assembled with the proposed design, has an effective stroke of about 4 m and very compact sizes of about 140 x 250 mm.

Figure 5. (**a**) Final design of the active part of the axis module and (**B**) detail of the cable chain and guide.

Another essential executive detail of the axis module is certainly the cable chain that guides and sustains the cables (the power supply and the command cable) during the motor working cycle. In fact, at the design velocity of 15 m/s, the cable has to be carefully unrolled to avoid incidents due to inertia of the not negligible cable masses. In addition, the cable must be protected by accidental collision with other equipment components during the operation. After different attempts, the solution proposed in figure 5 has been chosen. The chain is guided with a metallic guide profile and has a width lower than the support frame (to reduce the risk of accidental collisions). This avoids that, due to chain misalignments, the chain impacts against the frame that sustains the axis modules.
A general comment must be made for the whole axis module design: even though the axis module is assembled with standard industrial components, the working cycle of the e-BLAST exploits the top performance of each constitutive element. Especially the cable chain and linear bearing railways could have a shorter lifetime due to the demanding

velocities reached in the e-BLAST working cycles. This fact justify the systematic performance evaluation and the continuous check of mechanical components during the first experiments. In fact, the mechanical operation tolerances of the two motor sections need an accurate and precise assembly that could be influenced by the vibration generated by the impacting masses.

2.2 Mechanical support frame

The mechanical support frame has the same modular design of the axis modules and shares the same structural strategy: a series of modular high-stiffness aluminium profiles, connected with suitable joints. The final design of the e-BLAST simulator, as per November 2015, is reported in figure 6.

Figure 6. Final design of the e-BLAST facility at November 2015

The frame is characterized by a total height of about 3 m and a transverse dimension of less than 1 m. The axis modules can be easily translated vertically by simply changing the position of a series of joints. In practice, the specimen that can be tested in this configuration has a maximum height of 2.7 m and a width of 0.25 m. Obviously, the support frame can be changed to house specimens with different geometry by varying the number of axis modules and their position in order to accelerate different masses.
In the current configuration, the support frame is placed on a rigid steel base connected to the ELSA strong-floor. In addition, it is also connected to another steel plate fixed on the Reaction Wall to limit oscillations during the e-BLAST operation.

In order to check the axis modules performance (with the three axes) a test is run, where the e-BLAST accelerates three steel masses of about 50 kg each (figures 7). Each mass slides on two linear bearing railways (one is in common with the axis module) thanks to two carriages (figure 7a). To stop the masses at the end of the test a series of mechanical dumpers (aluminium tubes with a diameter of 90 mm and a thickness of 5 mm) has been placed on the Reaction-Wall plate to absorb the major part of the mass kinetic energy.

The three masses are pushed by the motor plates by mean of three aluminium sub-frames (a sort of mechanical hands), as shown in figure 7b. This frame serves two main purposes: it pushes the mass in its barycenter to limit moments and friction on the carriages, and it acts as an expendable element in case of possible mulfuctioning, safeguarding the more expensive motor elements.

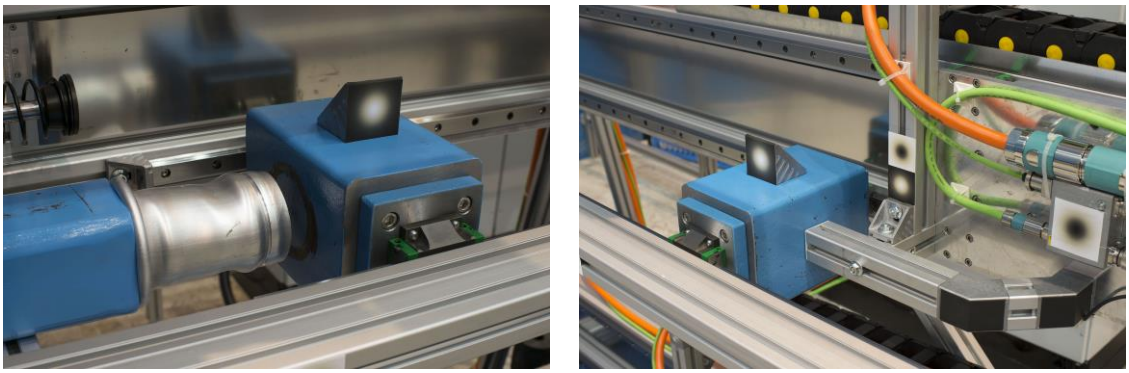

Figure 7. (**a**) Detail of the impacting mass and the target and (**B**) sub-frame that push the mass in the preliminary performances tests.

2.3 Instrumentation

In the present configuration the instrumentation adopted for the experiments is limited because no specimens are in place, and the axis modules performance can be efficiently deduced from the sensors, which are necessarily installed for the motor operation.
In fact a linear motor requires an accurate displacement sensor in order to operate with a closed-oop feedback strategy. The displacement sensor adopted in these firsts tests is the incremental linear encoder LIDA 287 (1 Vpp siynusoidal signal) with a precision of 2 micron and a length of 4 m (Annex C), shown in Figure 8a. In detail, the scanning head is rigidly connected to the motor plate using a calibrated spacer to ensure the correct working gap between the scanning head and the optical scale tape. In particular the narrow tollerance of the gap (0.45 mm) has been verified with a dial gauge along the whole motor stroke. Finally, the steel scale tape has been mounted using a series of aluminum extrusions to facilitate the assembly.

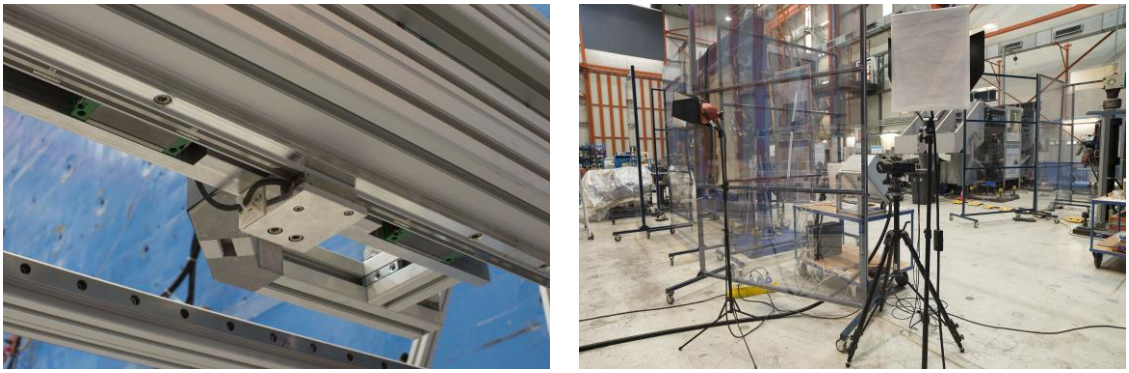

Figure 8. (**a**) Detail of linear encoder placed under the axis module and (**B**) the high-speed camera adopted during the test campaign.

The second piece of equipment adopted during the test campaign is a high-speed camera, an IDT Y4, that allows the recording of high-speed photo sequences during the tests, as shown in picture 8b. The camera greatly aids the comprehension of dynamic phenomena not easily visible at the naked human eye, as for example the motion of the

cable chain. In addition, applying a series of computational algorithms to the high-speed photo sequence, quantitative data concerning the motion of a series of targets can be extracted. This technique facilitates the study of the frame oscillations without placing any accelerometers at different points of the frame. The only "drawback" is requirement related to the fact that a suitable illumination (figure 8a) must be provided in order to acquire "frozen" frames and avoid blurred images.

2.4 Power supply and control unit

The e-BLAST is essentially a high-performance electrical motor and, for this reason, it is provided by a high power supply and control unit (figure 9a). The main electrical devices necessary for the operation of the three independent linear motors are housed in a single electrical cabinet. The power supply unit (120 kW three-phases) is common for the three motors and is directly connected to the global control unit of the system. The global control unit in then connected to the three single axis drives that supply and control each axis module. All motor power supply and control cables are directly connected to the cabinet, as is the centralized power cable. For all these very specific requirements, the cabinet has been manufactured and certified by an external supplier.

Figure 9. (**a**) Power supply and control electronics and (**B**) operator command console with PC interface for the motor programming (Starter program).

To communicate with the control unit inside the power cabinet an operator command console (figure 9b) has been designed and assembled. This simple console allows a series of motor operations to be done and commands the execution of the working cycles stored in the internal CPU. The operator console provides also the connection between the control unit and an external PC in order to set motor parameters as well the working cycle parameters. All these features are managed with the Starter software provided by Siemens.

2.5 Safety devices and procedures

The intrinsic dangerousness of the e-BLAST simulator, due to high electrical and mechanical power involved in the standard operation, requires a series of precautions and procedures to be taken in order to avoid injuries or incidents.
For what concerns the electrical risk all the electrical devices in the power cabinet have been assembled and certified by a qualified operator, as was also done for the connection of the cabinet to the ELSA power plant.
With reference to the risk connected to high velocity moving masses, three series of safety measures have been taken:

- Software limits. It is possible to set software displacement limits by means of the Starter software. Obviously, these limits work only with the control cabinet powered-on and they are not effective in case of accidental electrical interruption.

- Hardware limits. Even if the software limits were not properly set, the motion of each axis module would stop in a set of designed positions. This is obtained thanks to a series of electrical limit switches placed on both ends of the electrical stroke of the motor (figure 10a). An additional switch is adopted to give to the single axis the "home" position. Obviously, also this safety countermeasure is not effective during an electrical blackout.
- Mechanical dampers. Should both previous countermeasures fail, a third measure has been implemented for stopping the motors. This result can be reached with a series of mechanical dampers that can absorb all the kinetic energy of the motors. Figure 10b shows the solution adopted with the hydraulic dampers placed on the axis module extremity.

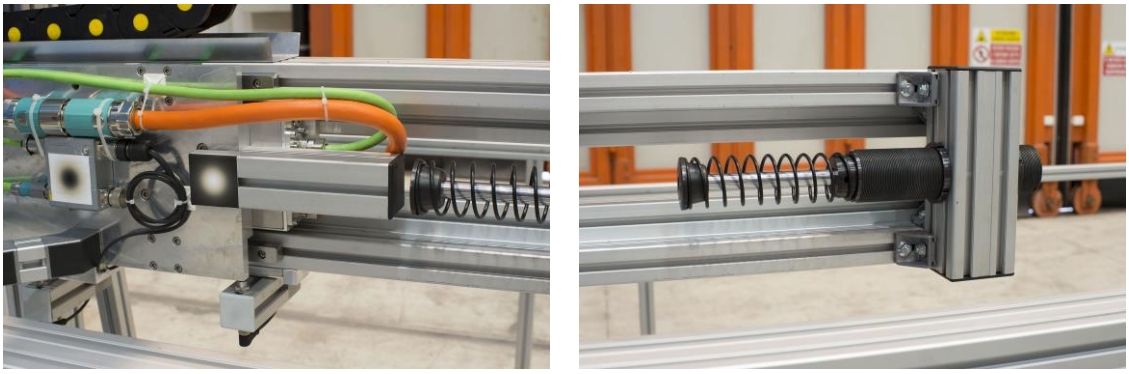

Figure 10. (**a**) Electrical limit switch and (**B**) hydraulic extremity damper.

In any case, it must be underlined that, due to the very low duration of the working cycle, it is not probable that an electrical blackout occurs during an e-BLAST test. In addition, the friction due to the bearing railway and the mutual magnetic forces between primary and secondary motor sections naturally decelerate the motors during a power supply interruption.

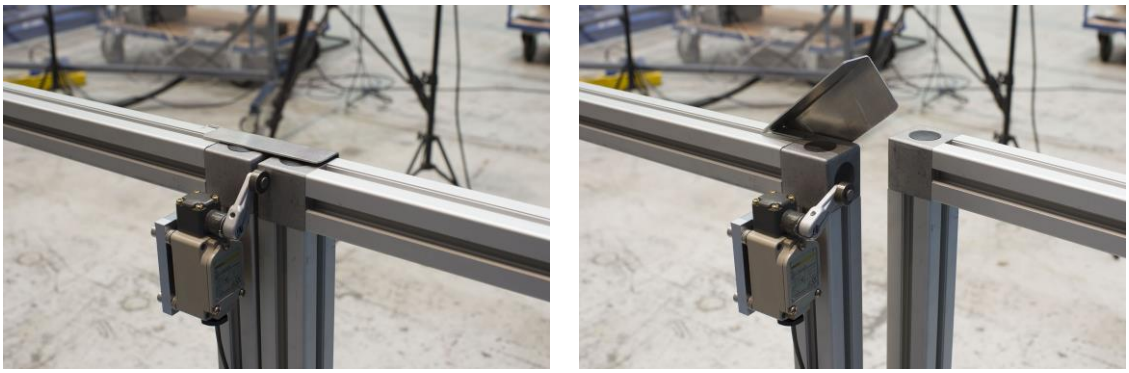

Figure 11. (**a**) Gate safety switch in closed and (**B**) open case.

Beyond the possibility of injuries due to un-controlled high-velocity moving motors, another possible sourse of risk lies in the standard operation of the e-blast. For this reason during an experiment nobody should be given access and be able to interact with the equipment. To avoid incidents also in the test setup, a safety fence has been placed around the e-BLAST at a distance of 1 m. The equipment access can be done only by means of two instrumented gates on the two sides of the rig. The opening of each gate causes an error in the command console that deliberetely makes impossible to start the equipment and, in addition, removes the electrical supply to the drives. After the closure

of the gates the error has to be reset by the command console before a new working cycle starts. This system consists of two switches mounted directly on the gates (figures 11), as commonly adopted in machine tools. The control cabinet is prearranged for a series of safety switches specifically designed for these purposes (safety gates, presence sensors, etc.).
Although the performance evaluation tests of e-BLAST does not involve materials able to produce flying debris, the operators are further protected by a series of transparent safety screens, visible in picture 8b. Furthermore, the operator console is placed in the opposite side with respect to the principal motion direction of the e-BLAST, where no accidental specimen debris can reach.
Finally, during the e-BLAST test campaign the access to the ELSA hall in proximity of the e-BLAST facility is restricted to the e-BLAST operators.

2.6 Advantages and disadvantages of e-BLAST

To conclude this section it is worth underlining some of the main advantages and disadvantages of the new e-BLAST compared with the previous spring-nitrogen driven blast simulator.

- Weight reduction. The main advantage of the e-BLAST, compared with the previous blast simulator (included the San Diego one), is definitely the equipment weight reduction. The g-BLAST, for example, has a weight of 1.5 tons and 3 tons of support frame. This huge mass makes difficult the assembly of more than one actuators, and it involves the manufacturing of heavy steel frames to support them. In addition, in this equipment the non-active accelerated mass is normally more than the useful impacting mass (in the g-BLAST more than 150 kg of piston rod) reducing the energy efficiency of this type of testing facility. On the other hand, in the e-BLAST the weight of the non-active mass (motor + plate + carriages) is less than 30 kg, thus reducing substantially the energy involved in a test. This feature implies a lighter support frame, which in this case can be manufactured with commercial structural aluminium profiles that can be assembled quickly ad-hoc for different testing setups.
- Modularity. As mentioned before, the modular design of e-BLAST is a successful strategy especially in view of testing different structural components. In fact, different components have normally various geometries that must be accommodated with the testing equipment. Heavy or fixed supporting structures and actuators are not able to provide this kind of versatility in the experimentation.
- Control performances. The control performance of an electrical linear motor is not comparable with any other mechanical actuator at the same velocity. This is due to the high stiffness control solution as no components are placed between the motor and the feedback sensor. In addition, differently from g-BLAST, the motor during the mass acceleration stroke is controlled until the detachment of the mass that can be done closed to the specimen, thus increasing the synchronisation of more than one impacts. Furthermore, two different control strategies are available. In the first one the three motors can work independently even though with the same target positions and start. Alternatively, a master axis module can be defined and the other two slave axes follow the actual position of the master axis.
- Easy test operation. The test operation of the e-BLAST is simple and very fast. The test can be performed a few seconds after the powering on of the electrical components.
- Time and displacement synchronisation. As mentioned before, the closed-loop feedback operation of the linear motors makes extremely simple and reliable the synchronisation between the axis modules. Considering that the maximum displacement error admitted in the acceleration stroke by the controller is 200 micron, at a velocity of 10 m/s it is equivalent to a time delay (between two axes) of

20 μs. This time delay is totally negligible compared with the positive phase duration of typical explosions of about 1-5 ms. Furthermore, not only synchronized impact can be generated but also particular delayed impacts to reproduce blast waves that arrive to the specimen at different times (no plane wave profiles).

- Low cost technology. Compared with other hydraulic or mixed hydraulic/pneumatic actuators the e-BLAST exploits a low-cost technology. Considering the infrastructure costs of the other facilities, such as the hydraulic power plant, the mechanical frame support or the triggering devices, the e-BLAST cost-attractive features are particularly attractive.

On the other hand, the e-BLAST compared with the previous generation blast simulator has one disadvantage: the capabilty of the e-BLAST in terms of velocity is nowadays limited to a maximum value of 15 m/s. This velocity allows the simulation of the effects of classical TNT explosions, but it poses limitations on the number of parameters that must be varied in order to reproduce the desired blast impulse.

3. Operational and performance evaluation tests

Following the discussion of the design and assembly of the e-BLAST facility, this section describes a series of tests for assessing the actual performance of the developed equipment.
Due to the maximum velocity compatible with the feedback sensor available for this test campaign, the maximum impacting mass velocity reached has been 10 m/s. Even though this value does not represent the full capability of the linear motor (approximately 15 m/s), it is a starting value that already allows a blast explosion profile to be reproduced using a suitable impacting mass. Obviously, increasing the maximum operation velocity of the equipment, a greater capability in terms of reproducible blast impulse can be achieved, and further investigations will be discussed below.
To compare directly the data obtained from the previous test campaigns with the g-BLAST actuator, a mass of 50 kg has been chosen to be accelerated.

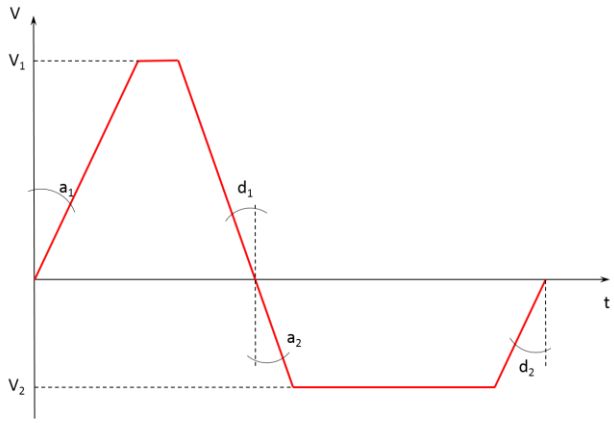

Figure 12. Example of e-BLAST working cycle.

After different attempts, the working cycle shown in figure 12 has been adopted for the acceleration of the impacting masses. The motor working cycle is characterized by a constant acceleration path (a1) until the maximum velocity (V_1) is reached and then a fast deceleration (d1) to zero velocity in a target position (x_0). At this point, the motor inverts its motion direction and comes back with a constant acceleration (a2) until an established velocity (V_2), and then constantly decelerates (d2) to stop at the home position. Obviously, in the tests that involve accelerated masses, when the motor starts its deceleration ramp (d_1), the mass and motor detach. In this way, during the impact the motor is sufficiently far away from the mass to avoid any damage.

Table 1. Working cycle table for the performance tests.

V [m/s]	Job	x_0	V [m/min]	a [%]	d [%]
6	1	2800	360	30	50
	2	(home)	180	50	30
7	1	2800	420	40	60
	2	(home)	210	60	40
8	1	2800	480	50	70
	2	(home)	240	70	50
9	1	2800	540	60	80
	2	(home)	270	80	60
10	1	2800	600	70	90
	2	(home)	300	90	70

The control strategy adopted during the tests consists of maintaining totally independent the three axis modules in the sense that they have the same working cycle implemented and the same starting signal but no other constraints during the execution of the working cycle. Despite the fact that this solution could have greater synchronicity errors (compared with a master-slave strategy), it guarantees more versatility in the test execution; in particular, in this way also delayed tests can be performed.
Table 1 reports the working cycles implemented in the motor controller (with the same nomenclature) for conducting the tests reported in the following. For each pair of maximum velocities, several parameters for the acceleration (job 1) and deceleration stroke (job 2) have to be defined. The acceleration and deceleration values are given as percentages of a nominal value of 50 m/s^2.
Two test series have been carried out and presented, a void test without any accelerated mass and the standard test with three 50 kg masses accelerated simultaneously.

3.1 Void tests (without additional masses)

A series of tests without any mass accelerated will be presented. These tests have been performed to check step-by-step the motor performance and the working cycles implemented in the motor controller. This phase is also suitable for identifying the correct control parameters for this range of velocities. In fact, the auto-tuning tool provided by Siemens seems to be not adequate in this kind of peculiar application (it returns control parameters too slow and conservative, suitable only for the standard low-performance industrial applications).
Only the results obtained from the fastest test (10 m/s) will be discussed in detail, because the other tests (reported synthetically in the Annex E) have the same trends. In addition, the 10 m/s test is the most demanding of the whole test campaign regarding the motors operation.

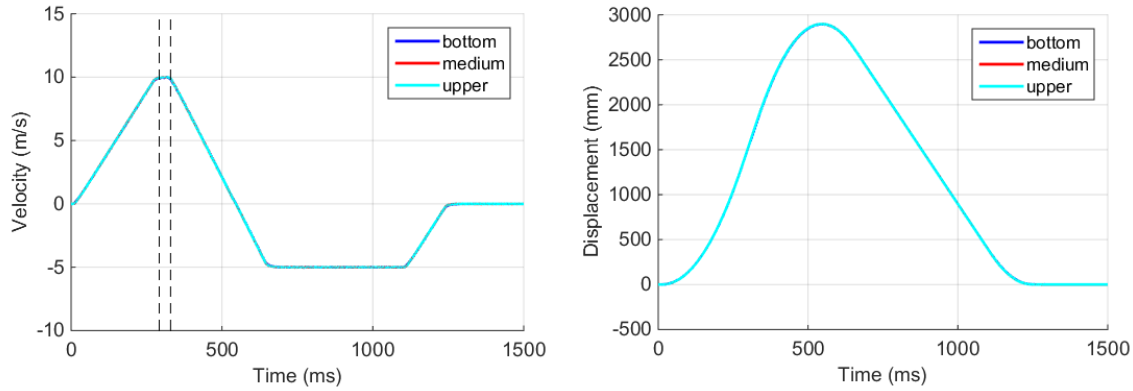

Figure 13. (**a**) Velocity and (**b**) displacement trends acquired by the linear motor encoders during the 10 m/s void test.

Figure 13 shows the velocity (figure 13a) and displacement (figure 13b) diagrams acquired by the linear motor encoders during the void test at 10 m/s with an optimized set of control parameters.
As it is simple to notice, it is impossible to observe any difference between the three linear axes at this scale and the actual working cycle is close to the theoretical one proposed in figure 12. The two dashed black lines in figure 3a delimitate the active portion (of maximum constant velocity) of the working cycle. Figure 14a shows, on the contrary, the control error during the prescribed working cycle. Obviously, the larger errors occur during the acceleration and deceleration phases whereas they are close to zero during the constant velocity phases. As in figure 13a, in pictures 14a the active constant velocity limits are reported (in black dashed lines) and the mean error in this region is reported in the legend. The differences between the target and the actual

positions of the three motors are less than 0.06 mm. This accuracy is amazing considering the velocity of controlled axis and corresponds to a time scale of the order of 6 μs (0.06 mm divided by 10 m/s).

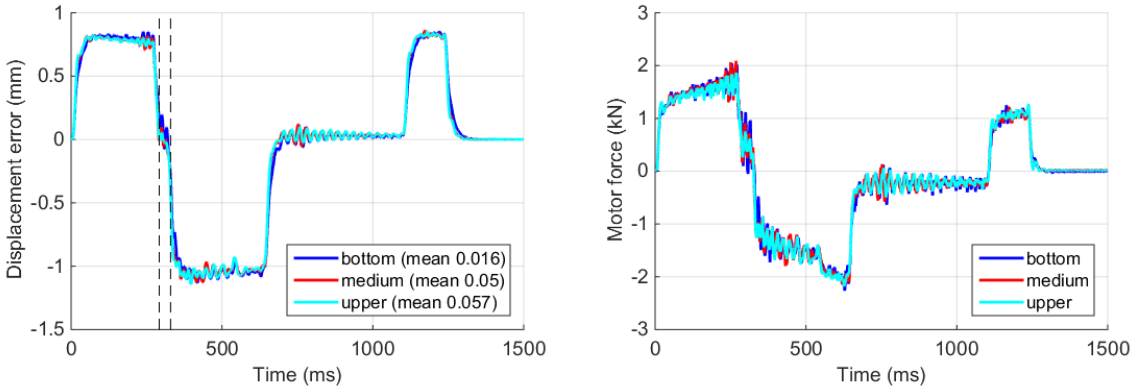

Figure 14. (**a**) Errors of the three axes in terms of displacement and (**b**) motor forces in 10 m/s during the void test

Figure 14b shows the motor forces applied by the primary sections to accelerate the motor itself, the motor plates and the cable-chains. As expected, the motor supplies higher forces during the acceleration/deceleration path while during the constant velocity phases the motor force drops to about zero. In fact, in these phases no inertia phenomena must be contrasted but only friction forces due to the railway system and the motor normal force component.
To validate these last considerations, figure 15 shows the motor forces recorded during tests of nominal maximum velocity of 1 m/s and 5 m/s, respectively. As it is simple to notice, the peak forces in the acceleration/ deceleration paths increase when the accelerations grow up. On the other hand, in the constant velocity phases the motor forces are, for all tests, lower than 500 N. The friction forces could probably be reduced by removing all lubricant seals mounted on the carriage, and which are not useful for this kind of application.
In addition, the evaluation of friction forces could be useful to judge the railway system and to prevent possible mounting misalignments that could threaten the motor performance.

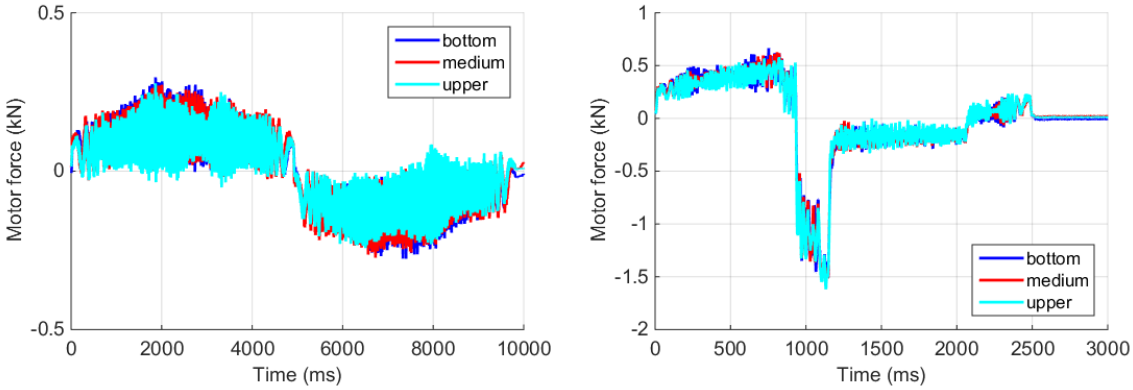

Figure 15. Motor forces at (**a**) 1 m/s and (**b**) 5 m/s void tests

Finally, figure 16 shows a high-speed photo sequence of the void test at 10 m/s. No unexpected behaviour of moving components has been observed (cable chains and

motors) and the computation of target positions on the support frames does not evidence any substantial oscillations.

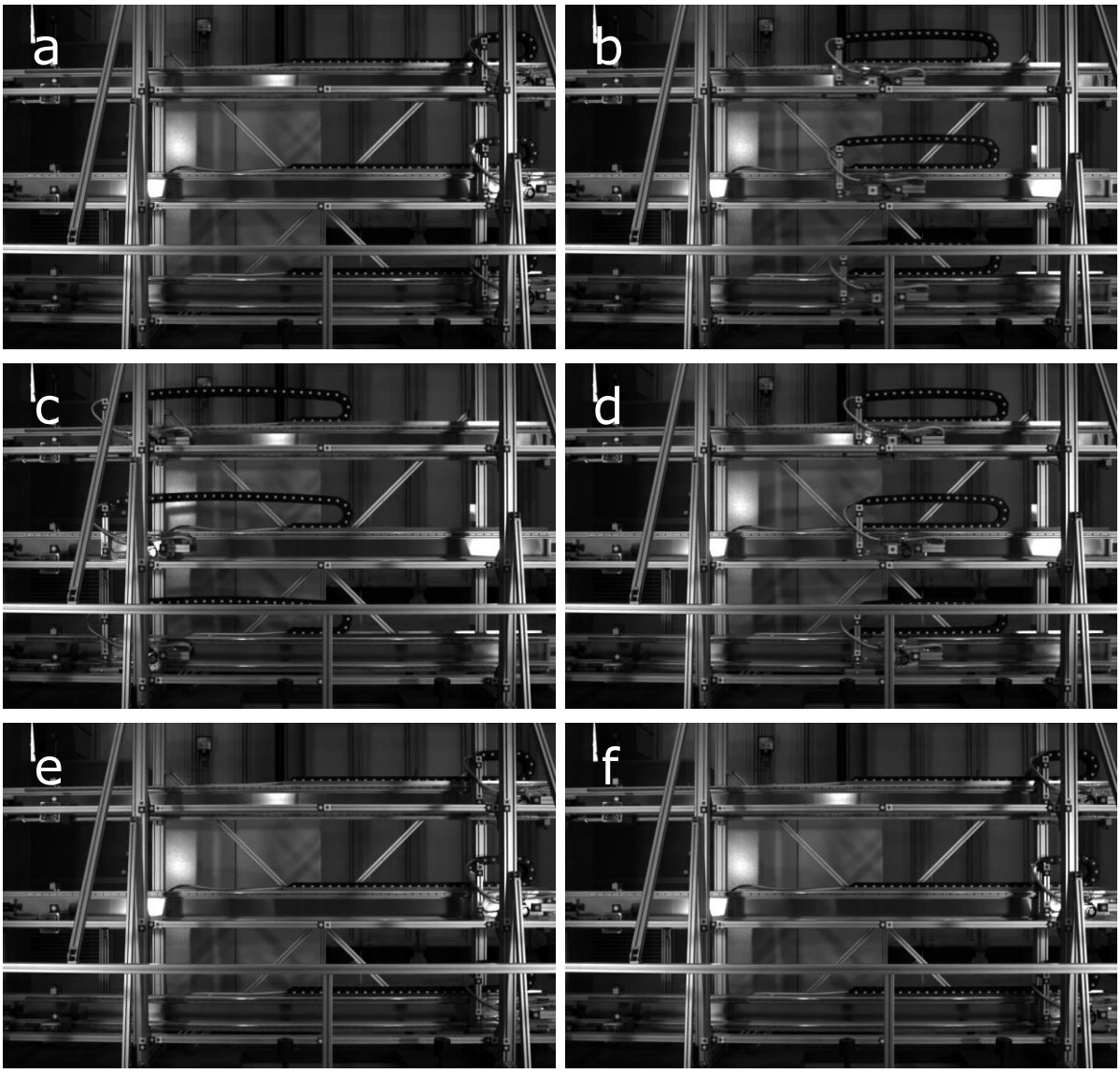

Figure 16. High-speed photo sequence of the 10 m/s void test

3.2 Accelerated masses tests (50 kg)

This paragraph presents main data acquired during the more representative performance tests of the e-BLAST. In detail, the three axis modules accelerate three masses of about 50 kg with the same working cycles reported in table 1. As for the void tests, only data concerning the most demanding test at 10 m/s will be presented (other tests reported synthetically in the Annex F). In addition, it must be underlined that only a reduced acceleration stroke of 2.8 m (instead of 4 m) has been used in order to have the possibility of increase the maximum velocity in further applications.
Figures 17 shows the same working cycle adopted in the void test and presented in the previous paragraph. Similarly, in this case it is impossible to notice considerable discrepancies between the three motor axes in what concerns both velocity (figure 17a) and displacement (figure 17b).
On the other hand, the analysis of the errors of the three motors along the working cycle allows some important considerations to be made. As expected, the errors in this more

demanding test substantially increase with respect to the void test. As reported in the graph legend, the mean error in the active constant velocity phase has grown to 0.2 mm.

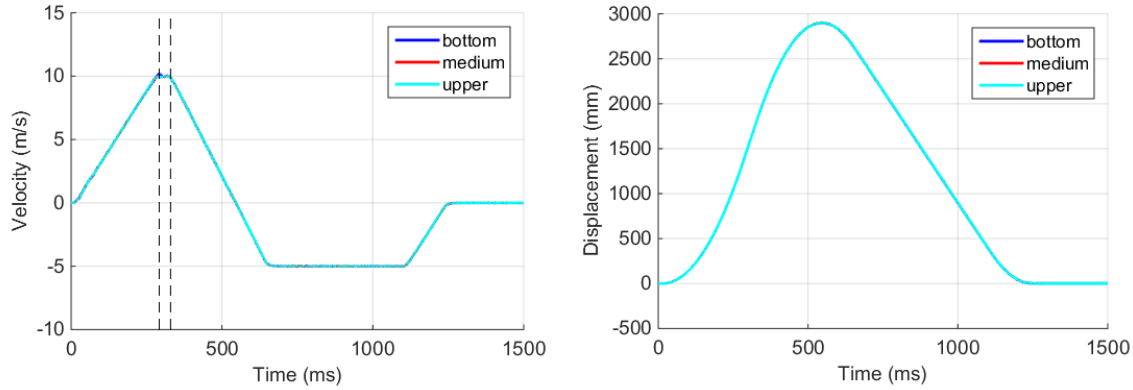

Figure 17. (**a**) Velocity and (**B**) displacement trends acquired by the linear motor encoders during the 10 m/s test with three 50 kg masses.

This value is, once more, an amazing example of motion control considering the velocity of the moving masses. The accuracy in terms of time is about 20 μs (0.2 mm divided by 10 m/s), which is a value barely reachable with other control techniques.

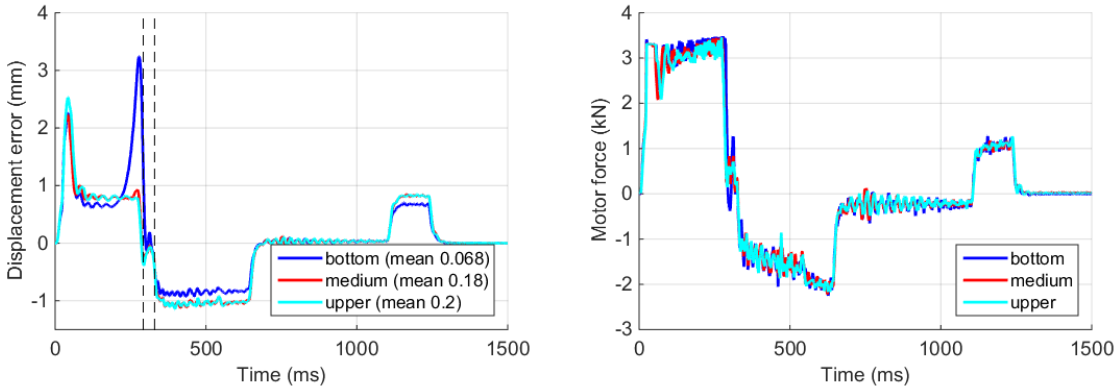

Figure 18. (**a**) Errors of the three axes in terms of displacement and (**b**) motor forces (test with three 50 kg masses).

It is interesting to notice that, as before, in the acceleration/deceleration paths the errors substantially increase. In addition, especially for the bottom motor axis at the end of the acceleration path the error increases abnormally due to the saturation of the motor force. This is probably due to a slightly higher friction coefficient of the railway bearing system. In any case, this situation is not desirable and in order to improve the control features it will be useful to increase the force limit (increasing the motor power consumption limit) or increase the motor acceleration stroke

Figure 18b highlights this last consideration: for each axis when the motor force saturates the control error dramatically increases because no additional correction can be applied to reduce the error.

Finally, figure 19 shows a high-speed photo sequence of the test at 10 m/s. Again, no unexpected behaviour of moving components has been observed (cable chains and motors) and the computation of target positions on the support frames does not evidence any substantial oscillations.

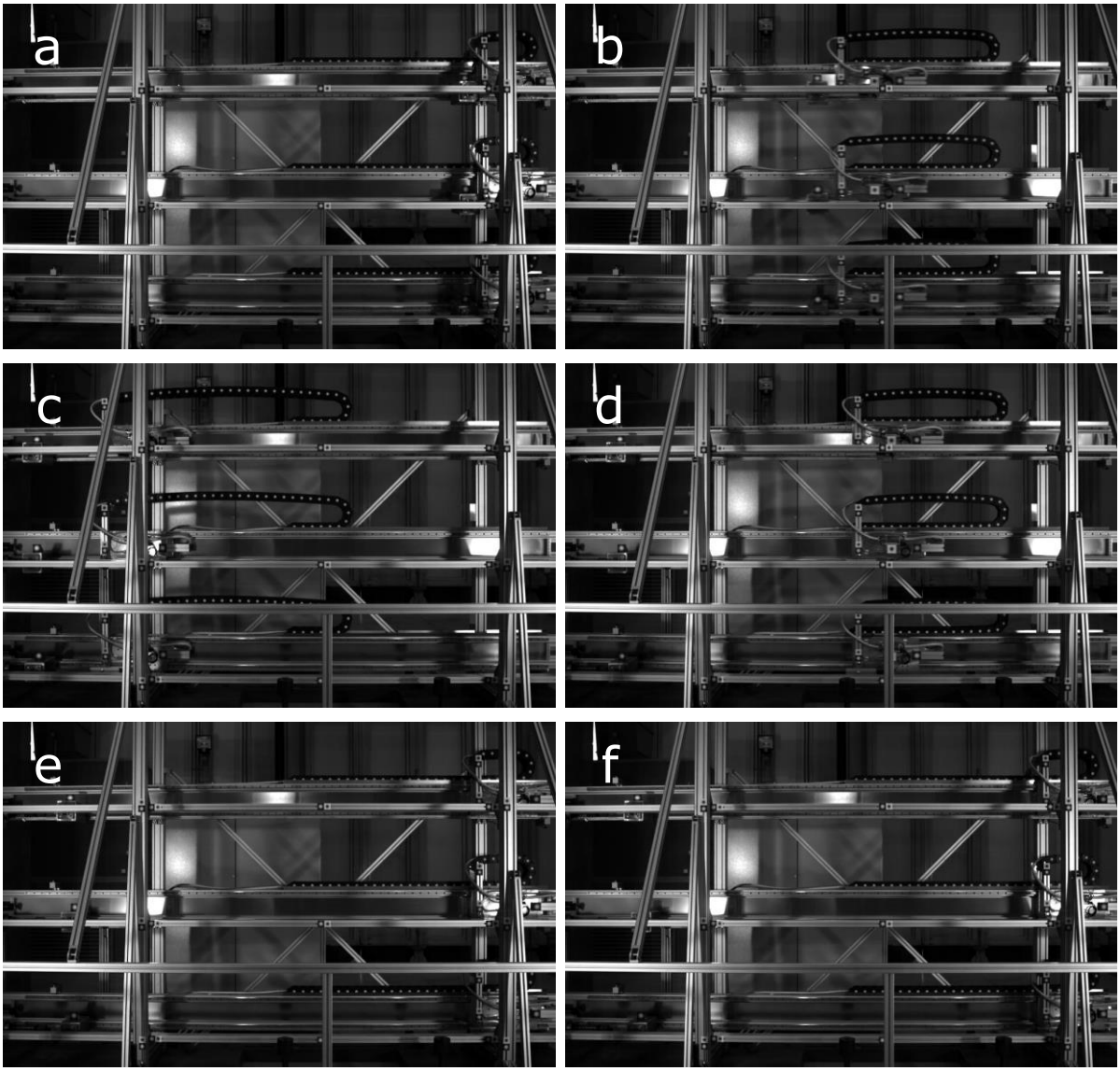

Figure 19. High-speed photo sequence of the 10 m/s test with 50 kg masses

4. Further developments

As mentioned before and demonstrated by the performance tests presented in the previous chapter, the e-BLAST facility fully meets the requirement necessary to perform blast simulation tests on structural components. Obviously, the full potential of an innovative testing rig cannot be achieved immediately, but it needs more time and several test campaigns and continuous improvements to be reached.
The essential improvements of the actual setup will be the substitution of the feedback displacement sensor with a faster linear encoder (with an operational velocity of 15 m/s). The sensor has been already identified and purchased. It is the linear encoder Renishaw RGH41 (datasheet in the Annex D) that has performance levels compatible with the linear motor limits. The change of the feedback sensor will imply some modifications in the scanning head aluminium support and in the alignment of the axis module.
Another possible improvement, for what concerns the axis module geometry, could be the complete redesign in order to adopt a twin configuration, as depicted in figure 2b. This configuration with two motors per axis has the great advantage of self-compensating the magnetic attraction forces between primary and secondary sections, thus reducing friction forces on the railway system doubling, and at the same time increasing the force capability of the axis. Obviously, such new design requires more motors, which constitute the more expensive part of the whole setup.
Moving away from the performance tests, the next step would be the execution of a large-scale test on a real structural component in the first semester of 2016. The equipment support frame, as currently designed, is suitable for the characterization of a column structural element (1D element), as shown in the sketch in figure 19

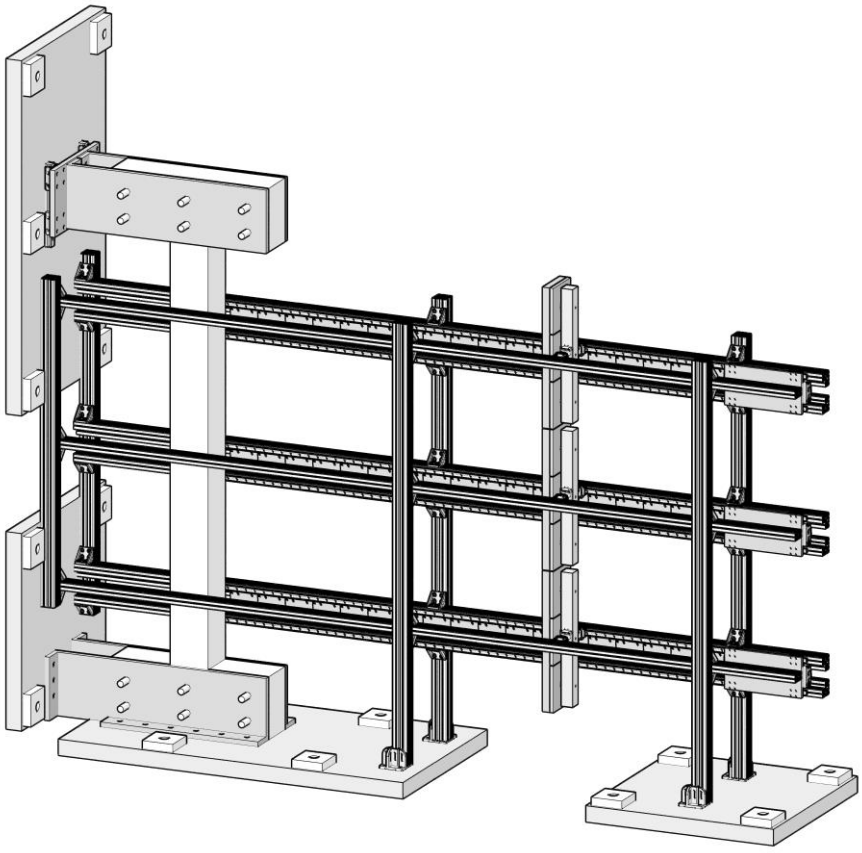

Figure 19. Possible large-scale dynamic test on column element with e-BLAST in 2016.

Using three masses with the same geometry as that adopted in [5], a column with a span of 2.7 m could be uniformly blast loaded on one side. In addition, a vertical pre-stress could be applied to the column to reproduce effectively a more representative situation (simulating the weight of the over-structure). With the same setup, both reinforced concrete and metallic columns could be tested. Introducing a delay between the impacts of the different masses, non-plane blast wave profiles could be generated, thus reproducing the effects of an explosive charge placed, for example, very close to the bottom of a tall column specimen.
The subsequent step of a test on bi-dimensional structural elements (walls, glass-panels etc.) will be kept into account after the tests on linear elements (columns or beams) have been successfully conducted.

5 Conclusions

This report presents in detail the philosophy of design and the assembly of the new Electrical Blast Simulator (e-BLAST) facility, along with a series of preliminary tests carried out in the ELSA laboratory in order to assess its performance. The e-BLAST facility involves the development of an apparatus able to reproduce the effects of a blast pressure wave on large-scale structural components (such as columns, walls, etc.) with the objective of improving their strength under these severe loading situations.

As demonstrated, differently from the prototype developed in previous projects concerning hydraulic/gas driven blast actuators, the e-BLAST exploits a recent technology that appears to be particularly suitable and promising in this research field. Specifically, synchronous electrical linear motors have been adopted for accelarating the impacting masses, thus allowing to design a more effective, versatile and low-cost facility. The whole equipment design has been thoroughly investigated together with the motivations and the consequences of the strategy adopted.

A series of operational tests carried out at a maximum impact velocity of 10 m/s (limit imposed by the present feedback sensors) has been carried out in order to assess the actual equipment performance in terms of acceleration capabilities. The tests have been performed with three impacting masses of about 50 kg and an acceleration stroke of about 3 m. The synchronization among the motion of the different masses seems to be fully adequate for the simulation of blast wave phenomena and the equipment operation is substantially simplified, compared with previous generation of blast simulator prototypes.

Finally a series of further modifications and improvements have been indicated aiming at upgrading the capabilities of the apparatus and satisfying the needs and requirements of future experimentation.

References

[1] Peroni M, Solomos G, Viaccoz B, Pegon P, Magonette G. Blast Simulator Setup Requirements. Administrative Arrangement No JRC 32253-2011 with DG-HOME Activity A5 - Blast Simulation Technology Development Deliverables 5.3, 5.4. EUR 26018. Luxembourg (Luxembourg): Publication Office of the European Union; 2013. JRC79971

[2] Peroni M, Solomos G, Caverzan A, Pegon P, Viaccoz B. Blast Simulator project: First tests on reinforced concrete beams. EUR 27051. Luxembourg (Luxembourg): Publications Office of the European Union; 2014. JRC94162

[3] Peroni M., Solomos G., Caverzan A., Larcher M. And Valsamos G. Assessment of dynamic mechanical behaviour of reinforced concrete beams using a blast simulator. EPJ Web of Conferences 94, 2015

[4] Larcher M, Valsamos G, Solomos G. Numerical material modelling for the blast actuator. EUR 26407. Luxembourg (Luxembourg): Publications Office of the European Union; 2013. JRC86348

[5] Valsamos G, Larcher M, Solomos G, Anthoine A. Numerical simulations in support of the blast actuator development. EUR 26430. Luxembourg (Luxembourg): Publications Office of the European Union; 2013. JRC86464

List of figures

List of tables

Annex A

1FN3300-3WG00-0xA1 motor data

1FN3300-3WG00-0xA1			
Technical specifications	**Short designation**	**Unit**	**Value**
Supplementary conditions			
DC link voltage	U_{ZK}	V	600
Water cooling inlet temperature	T_{VORL}	°C	35
Rated temperature	T_N	°C	120
Rated data			
Rated force	F_N	N	1840
Rated current	I_N	A	50
Maximum velocity at rated force	$v_{MAX,FN}$	m/min	836
Rated power loss	$P_{V,N}$	W	1370
Limit data			
Maximum force	F_{MAX}	N	5170
Maximum current	I_{MAX}	A	154.9
Maximum velocity at maximum force	$v_{MAX,FMAX}$	m/min	383
Maximum electric power input	$P_{EL,MAX}$	W	46180
Stall force	F_0*	N	1299
Stall current	I_0*	A	35.4
Physical constants			
Force constant at 20 °C	$k_{F,20}$	N/A	37
Voltage constant	k_E	Vs/m	12.2
Motor constant at 20 °C	$k_{M,20}$	$N/W^{0.5}$	58.6
Motor winding resistance at 20 °C	$R_{STR,20}$	Ω	0.1
Phase inductance	L_{STR}	mH	1.5
Attraction force	F_A	N	10300
Thermal time constant	t_{TH}	s	120
Pole width	τ_M	mm	23
Mass of the primary section	m_P	kg	17
Mass of the primary section with precision cooler	$m_{P,P}$	kg	18.4
Mass of a secondary section	m_S	kg	2.4
Mass of a secondary section with cooling sections	$m_{S,P}$	kg	2.6

1FN3300-3WG00-0xA1			
Technical specifications	**Short designation**	**Unit**	**Value**
Primary section main cooler data			
Maximum dissipated heat output	$Q_{P,H,MAX}$	W	1370
Recommended minimum volume flow	$V_{P,H,MIN}$	l/min	4.5
Cooling medium temperature increase	$\Delta T_{P,H}$	K	4.4
Pressure drop	$\Delta p_{P,H}$	bar	0.56
Primary section precision cooler data			
Maximum dissipated heat output	$Q_{P,P,MAX}$	W	50
Recommended minimum volume flow	$V_{P,P,MIN}$	l/min	4.5
Pressure drop	$\Delta p_{P,P}$	bar	0.53
Secondary section cooling data			
Maximum dissipated heat output	$Q_{S,MAX}$	W	136
Recommended minimum volume flow	$V_{S,MIN}$	l/min	4.5
Pressure drop per meter of secondary section cooling	Δp_S	bar	0.12
Pressure drop per combi distributor	Δp_{KV}	bar	0.53
Pressure drop per coupling point	Δp_{KS}	bar	0.39

1FN3300-3WG00-0xA1 characteristic curves

Force characteristics

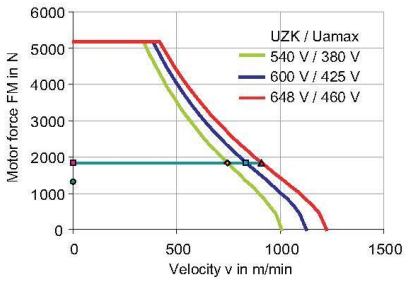

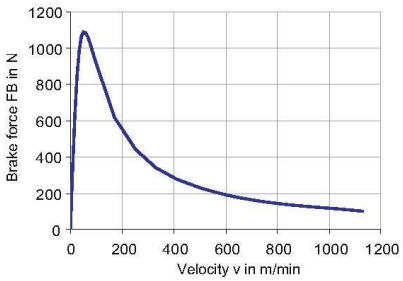

Primary section main cooler characteristics

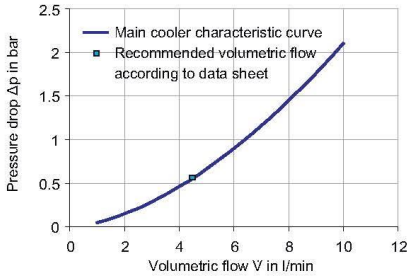

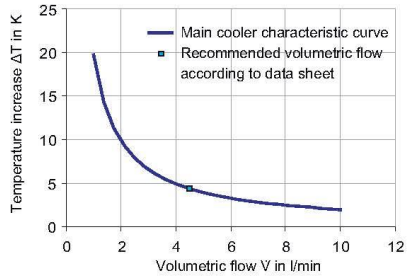

Pressure drop characteristics for the primary section precision cooler and the secondary section cooling system

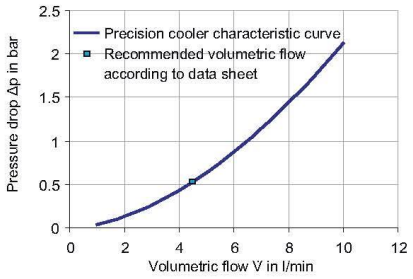

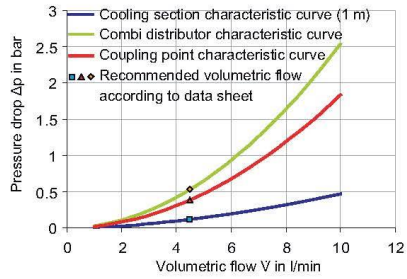

Annex B

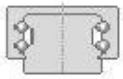

Guideways TKVD25-U (Series TKVD..-U)

for linear ball bearing unit and four-row linear recirculating ball guidance system, for screw mounting from below

The datasheet is only an overview of dimensions and basic load ratings of the selected product. Please always observe all the guidelines in these overview pages. Further information is given on many products under the menu item "Description". You can also order comprehensive information via the Catalogue ordering system (http://www.ina.de/content.ina.de/en/mediathek/library/library.jsp) or by telephone on +49 (91 32) 82 - 28 97.

h	18,7	mm	
b	23	mm	Tolerance: -0,005 / -0,03
l_{max}	2960	mm	Maximum length of single-piece guideways; longer guideways are supplied in several sections and are marked accordingly. Maximum single-piece guideway length of 6 m by agreement.
1)			Locating face
2)			Marking
$a_{L\,max}$	53	mm	a L and a R are dependent on the length l max of the guideway
$a_{L\,min}$	20	mm	a L and a R are dependent on the length l max of the guideway
$a_{R\,max}$	53	mm	a L and a R are dependent on the length l max of the guideway
$a_{R\,min}$	20	mm	a L and a R are dependent on the length l max of the guideway
G_1	M6		For screws to DIN ISO 4762-12.9 Max. tightening torque in Nm: M3 = 2,5 M4 = 5 M5 = 10 M6 = 17 M8 = 41 M12 = 140 M14 = 220 M16 = 340 If there is a possibility of settling, the fixing screws should be secured against rotation
j_L	60	mm	
t_r	12	mm	

ms	2,7 kg/m	Mass of guideway

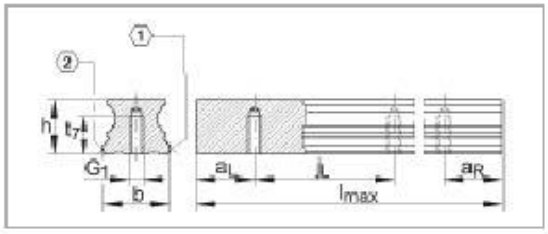

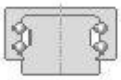

Carriages KWVE25-B (Series KWVE..-B)

standard carriage, four-row, full complement ball set

The datasheet is only an overview of dimensions and basic load ratings of the selected product. Please always observe all the guidelines in these overview pages. Further information is given on many products under the menu item "Description". You can also order comprehensive information via the Catalogue ordering system (http://www.ina.de/content.ina.de/en/mediathek/library/library.jsp) or by telephone on +49 (91 32) 82 - 28 97.

H	36	mm	
B	70	mm	
L	83,3	mm	
1)			Locating face
2)			Marking
3)			Lubrication nipple with tapered head to DIN 71 412-B M6 is supplied loose
A_1	23,5	mm	
A_2	6,5	mm	
A_3	11	mm	
A_4	6,5	mm	
$a_{L\,max}$	53	mm	a L and a R are dependent on the length l max of the guideway
$a_{L\,min}$	20	mm	a L and a R are dependent on the length l max of the guideway
$a_{R\,max}$	53	mm	a L and a R are dependent on the length l max of the guideway
$a_{R\,min}$	20	mm	a L and a R are dependent on the length l max of the guideway
b	23	mm	Tolerance: -0,005 / -0,03
G_2	M8		For screws to DIN ISO 4762-12.9 Max. tightening torque in Nm: M5 = 5,8 M6 = 10 M8 = 24 M10 = 41 M12 = 83 M14 = 140 If there is a possibility of settling, the fixing screws should be secured against rotation.

h	18,7 mm	
H_1	5,1 mm	
h_1	8,7 mm	
H_4	10,9 mm	
H_5	5,25 mm	
J_B	57 mm	
J_L	45 mm	
j_L	60 mm	
J_{Le}	12,85 mm	
J_{Lz}	40 mm	
K_1	M6	For screws to DIN ISO 4762-12.9 Max. tightening torque in Nm: M3 = 2,5 M4 = 5 M5 = 10 M6 = 17 M8 = 41 M10 = 83 M12 = 140 M14 = 220 M16 = 340 If there is a possibility of settling, the fixing screws should be secured against rotation
K_3	M6	For screws to DIN ISO 4762-12.9 Max. tightening torque in Nm: M3 = 2,5 M4 = 5 M5 = 10 M6 = 17 M8 = 41 M10 = 83 M12 = 140 M14 = 220 M16 = 340 If there is a possibility of settling, the fixing screws should be secured against rotation
K_6	M6	For screws to DIN ISO 4762-12.9 Max. tightening torque in Nm: M3 = 2,5 M4 = 5 M5 = 10 M6 = 17 M8 = 41 M10 = 83 M12 = 140 M14 = 220 M16 = 340

			If there is a possibility of settling, the fixing screws should be secured against rotation
L_1	60,7	mm	
l_{max}	2960	mm	Maximum length of single-piece guideways; longer guideways are supplied in several sections and are marked accordingly. Maximum single-piece guideway length of 6 m by agreement.
L_s	1,65	mm	
N_3	5,5	mm	Maximum permissible screw depth for lubrication connector: 7 mm
N_4	5,6	mm	Maximum permissible screw depth for lubrication connector: 7 mm
S	0,8	mm	
Ts	10	mm	
Te	10	mm	
We	6	mm	Width across flats
m_W	0,68	kg	Mass of carriage
m_S	2,7	kg/m	Mass of guideway
			Calculation of basic load rating according to DIN 636, increased basic dynamic load rating possible on the basis of practical experience.
C	17900	N	Basic dynamic load rating
Co	37000	N	Basic static load rating
M_{oX}	510	Nm	Static moment rating about X axis
M_{oY}	395	Nm	Static moment rating about Y axis
M_{oZ}	395	Nm	Static moment rating about Z axis

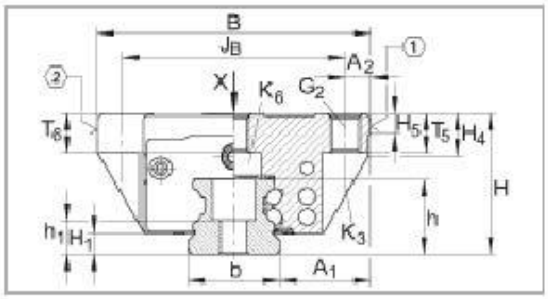

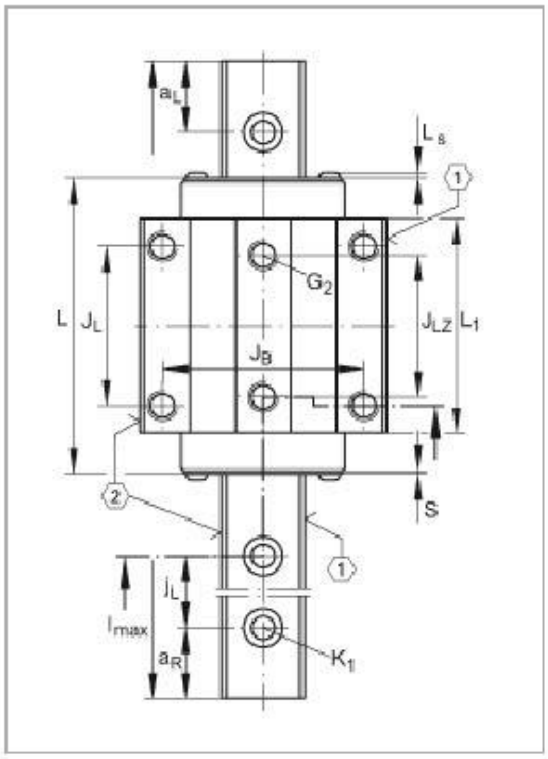
a_L
L_s
1
G_2
L
J_L
J_B
J_{LZ}
L_1
2
S
1
J_L
l_{max}
a_R
K_1

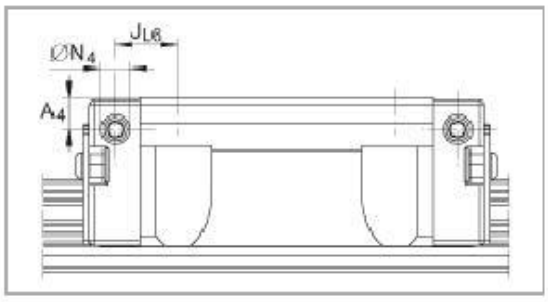
J_{L6}
$\varnothing N_4$
A_4

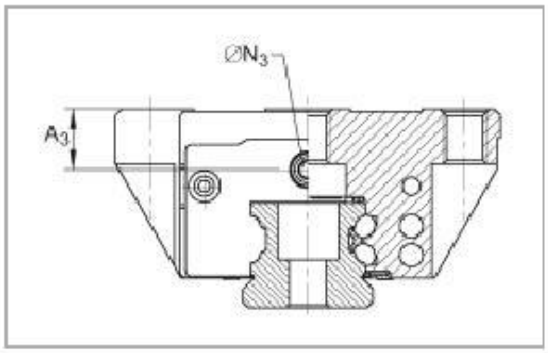

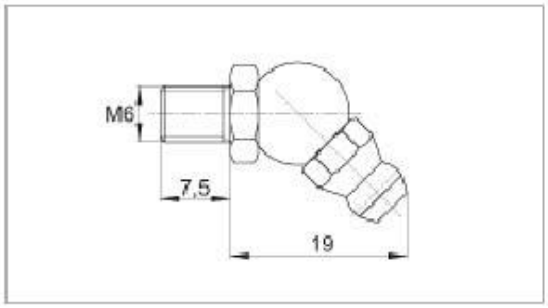

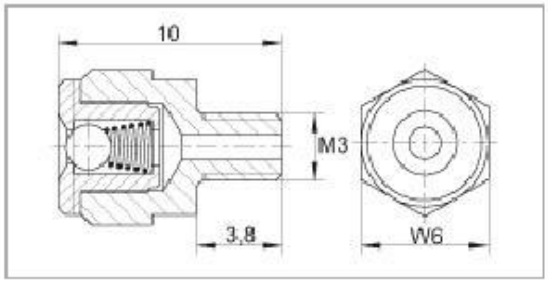

20.11.2015 11:30 5

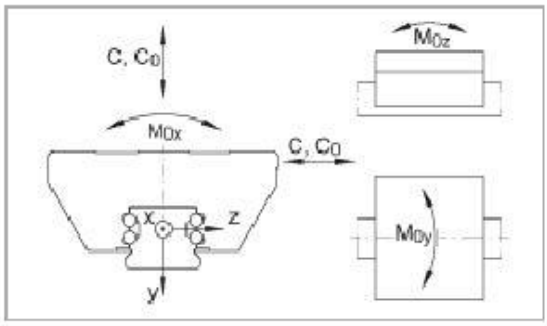

20.11.2015 11:30 6

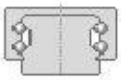

Carriages KWVE25-B-S (Series KWVE..-B-S)

narrow carriage, four-row; corrosion-resistant design possible

The datasheet is only an overview of dimensions and basic load ratings of the selected product. Please always observe all the guidelines in these overview pages. Further information is given on many products under the menu item "Description". You can also order comprehensive information via the Catalogue ordering system (http://www.ina.de/content.ina.de/en/mediathek/library/library.jsp) or by telephone on +49 (91 32) 82 - 28 97.

H	36	mm	
B	48	mm	
L	83,3	mm	
1)			Locating face
2)			Marking
3)			Lubrication nipple with tapered head to DIN 71 412-B M6 is supplied loose
A_1	12,5	mm	
A_2	6,5	mm	
A_3	11	mm	
A_4	6,5	mm	
$a_{L\,max}$	53	mm	a L and a R are dependent on the length l max of the guideway
$a_{L\,min}$	20	mm	a L and a R are dependent on the length l max of the guideway
$a_{R\,max}$	53	mm	a L and a R are dependent on the length l max of the guideway
$a_{R\,min}$	20	mm	a L and a R are dependent on the length l max of the guideway
b	23	mm	Tolerance: -0,005 / -0,03
G_2	M6		For screws to DIN ISO 4762-12.9 Max. tightening torque in Nm: M4 = 5 M5 = 10 M6 = 17 M8 = 41 M10 = 83 M12 = 140

			M14 = 220 If there is a possibility of settling, the fixing screws should be secured against rotation.
h	18,7	mm	
H_1	5,1	mm	
h_1	8,7	mm	
H_5	5,25	mm	
J_B	35	mm	
J_L	35	mm	
j_L	60	mm	
J_{US}	17,9	mm	
K_1	M6		For screws to DIN ISO 4762-12.9 Max. tightening torque in Nm: M3 = 2,5 M4 = 5 M5 = 10 M6 = 17 M8 = 41 M10 = 83 M12 = 140 M14 = 220 M16 = 340 If there is a possibility of settling, the fixing screws should be secured against rotation
L_1	60,7	mm	
l_{max}	2960	mm	Maximum length of single-piece guideways; longer guideways are supplied in several sections and are marked accordingly. Maximum single-piece guideway length of 6 m by agreement.
L_S	1,65	mm	
N_3	5,5	mm	Maximum permissible screw depth for lubrication connector: 7 mm
N_4	5,6	mm	Maximum permissible screw depth for lubrication connector: 7 mm
S	0,8	mm	
T_S	10	mm	
W_S	6	mm	Width across flats
m_W	0,56	kg	Mass of carriage
m_S	2,7	kg/m	Mass of guideway
			Calculation of basic load rating according to DIN 636, increased basic dynamic load rating possible on the basis of practical experience.
C	17900	N	Basic dynamic load rating
Co	37000	N	Basic static load rating

M_{0x}	510	Nm	Static moment rating about X axis
M_{0y}	395	Nm	Static moment rating about Y axis
M_{0z}	395	Nm	Static moment rating about Z axis

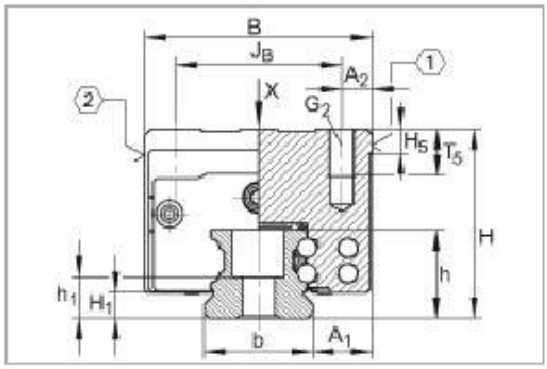

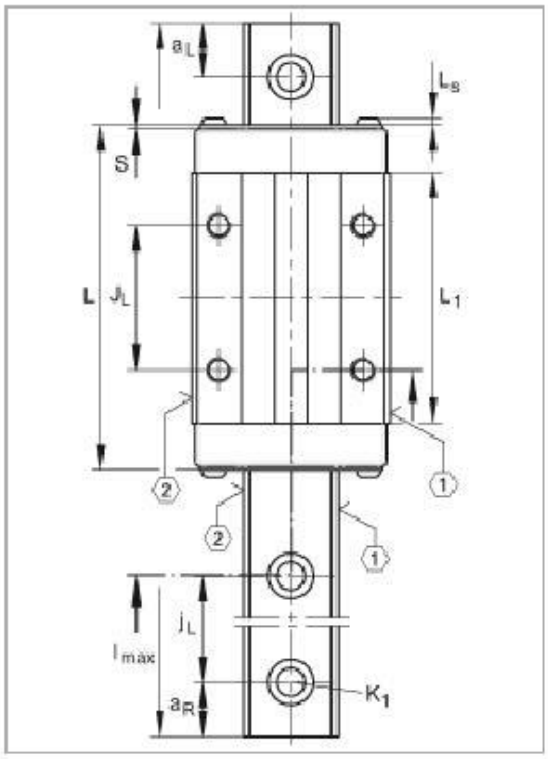
a_L
L_s
S
L
j_L
L_1
2
2
1
1
j_L
l_{max}
a_R
K_1

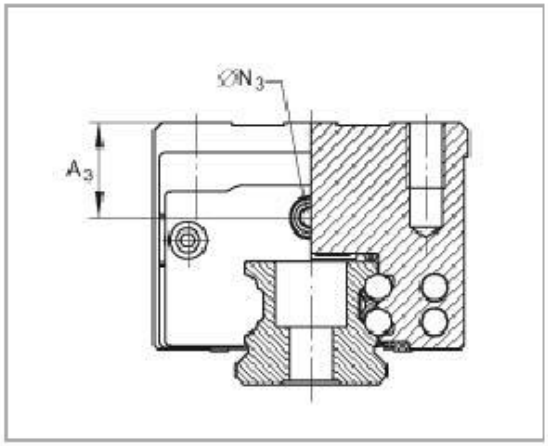
$\varnothing N_3$
A_3

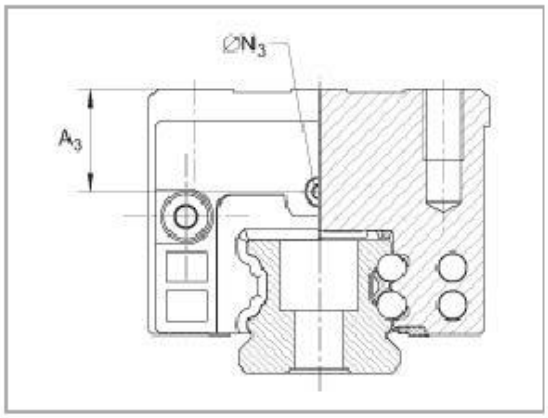

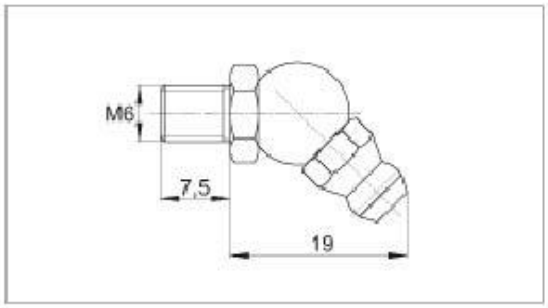

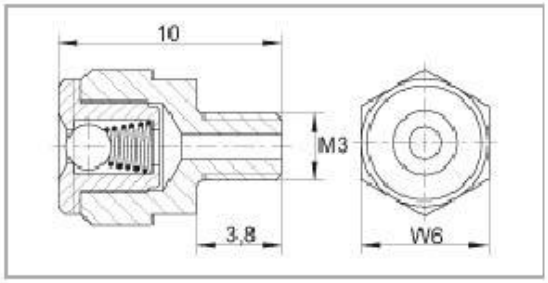

20.11.2015 11:29 5

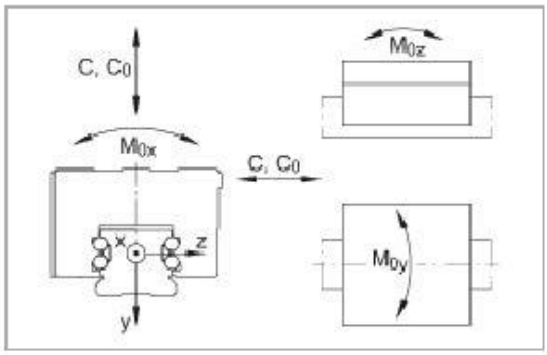
C, C0
M0x
C, C0
M0z
M0y
x
z
y

Annex C

LIDA 277, LIDA 287

Incremental linear encoder with large mounting tolerance

- **For measuring steps to 0.5 µm**
- **Scale tape cut from roll**
- **Steel scale-tape is drawn into adhesive aluminum extrusions and fixed**
- **Integrated status display with three-color LED**
- **Consists of scale and scanning head**

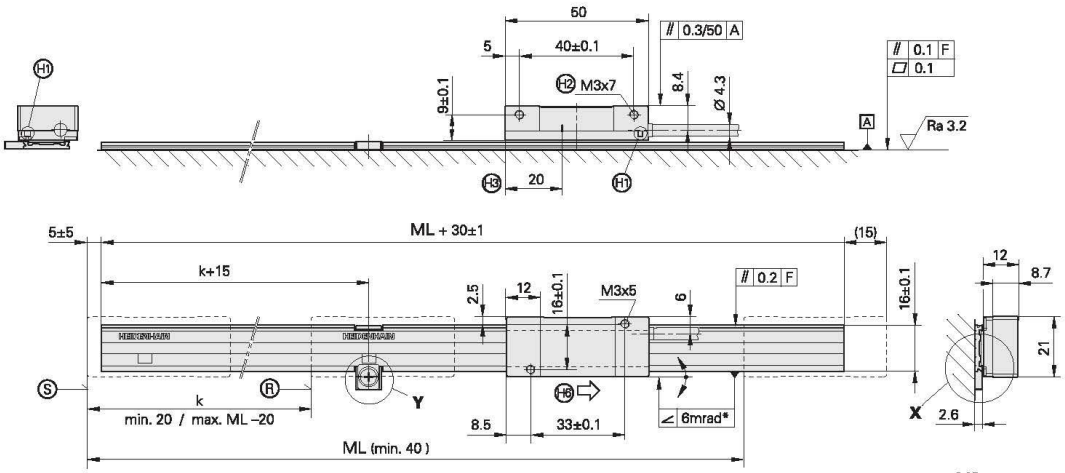

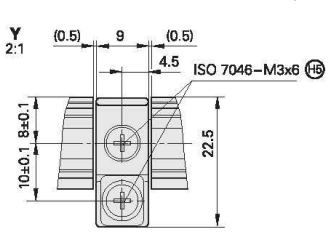

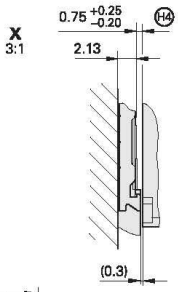

Possibilities for mounting the scanning head

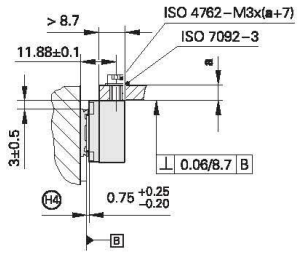

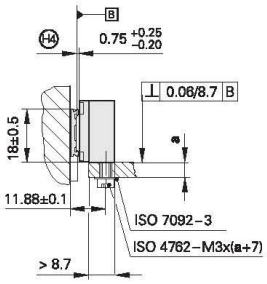

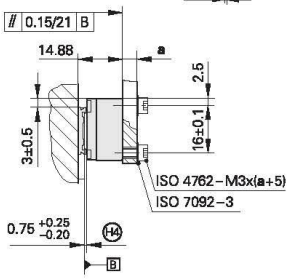

mm

Tolerancing ISO 8015
ISO 2768 - m H
< 6 mm: ±0.2 mm

* = Max. change during operation
F = Machine guideway
Ⓡ = Reference mark
Ⓛ = Scale tape length
Ⓢ = Beginning of measuring length (ML)
Ⓗ1 = LED (integrated checking of the mounting)
Ⓗ2 = Thread at both ends
Ⓗ3 = Position of reference mark relative to scanning head
Ⓗ4 = Mounting clearance between scale and scanning head
Ⓗ5 = Mating threaded hole, M3, 5 mm deep
Ⓗ6 = Direction of scanning unit motion for output signals in accordance with interface description

Reference mark:
k = Any position of the selected reference mark starting from the beginning of the measuring length (depends on the length of cut)

52

Linear scale	LIDA 207
Measuring standard Coefficient of linear expansion	Steel scale tape, grating period 200 µm $\alpha_{therm} \approx 10 \cdot 10^{-6}\ K^{-1}$
Accuracy grade	± 15 µm
Scale tape cut from roll*	3 m, 5 m, 10 m
Reference marks	Selectable every 100 mm
Weight Scale tape Scale-tape carrier	20 g/m 70 g/m

Scanning head	AK LIDA 28	AK LIDA 27		
Interface	∿ 1 V_{PP}	⊓⊔ TTL		
Integrated interpolation* Signal period	– 200 µm	10-fold 20 µm	50-fold 4 µm	100-fold 2 µm
Cut-off frequency Scanning frequency Edge separation a	≥ 50 kHz – –	– ≥ 50 kHz ≥ 0.465 µs	– ≤ 25 kHz ≥ 0.175 µs	– ≤ 12.5 kHz ≥ 0.175 µs
Traversing speed	≤ 600 m/min		≤ 300 m/min	≤ 150 m/min
Electrical connection*	Cable, 1 m or 3 m with 15-pin D-sub connector (male)			
Cable length	See interface description, but ≤ 30 m (with HEIDENHAIN cable)			
Voltage supply	5 V DC ± 0.25 V	5 V DC ± 0.25 V		
Current consumption	< 155 mA	< 165 mA (without load)		
Vibration 55 Hz to 2000 Hz **Shock** 11 ms	≤ 200 m/s^2 (EN 60068-2-6) ≤ 500 m/s^2 (EN 60068-2-27)			
Operating temperature	–10 °C to 70 °C			
Weight Scanning head Connecting cable Connector	20 g (without connecting cable) 30 g/m 32 g			

* Please select when ordering

Annex D

Scheda tecnica
L-9517-9144-03-D

RENISHAW
apply innovation™

Lettori RGH41

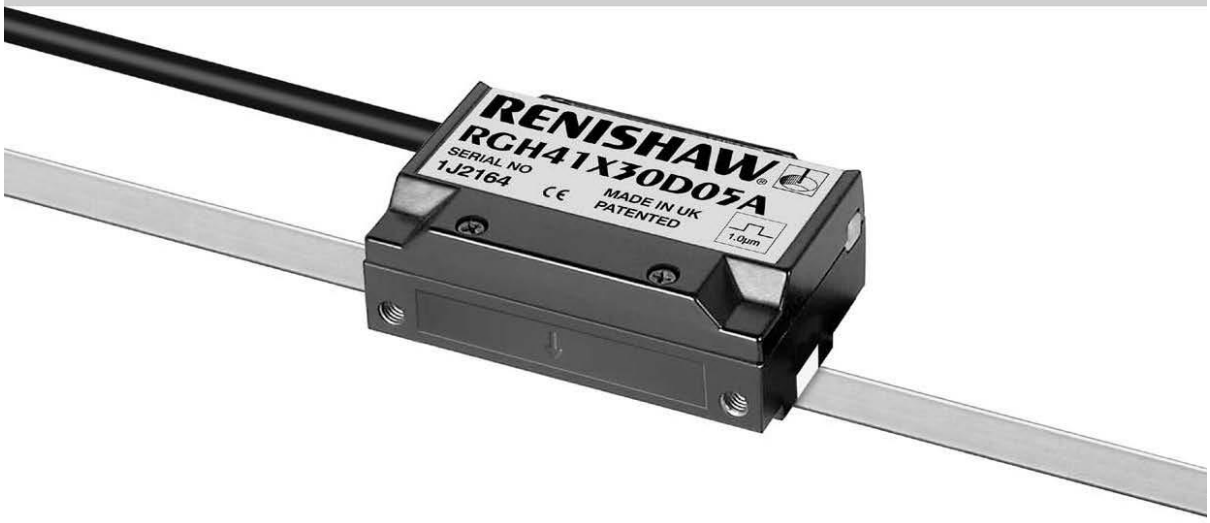

I lettori Renishaw da 40 µm della serie RGH41 offrono tutti i vantaggi dei sistemi di encoder lineari RG2 da 20 µm: scala a nastro a riflessione, ottiche di filtraggio brevettate, LED di allineamento, buona resistenza alla polvere e velocità elevata.

Questi lettori compatti con interpolazione integrale allargano la gamma di risoluzioni per soddisfare le richieste di un maggior numero di applicazioni, mentre la velocità elevata consente di incrementare la produttività del sistema dell'utente finale.

Il sistema RGH41 a 40 µm aumenta le già notevoli tolleranze di setup del sistema RG2, mantenendone al contempo la rinomata immunità alla contaminazione.

Per una maggiore flessibilità, è incluso di serie un doppio sensore di limite che consente di avere segnali dedicati per ciascuna indicazione di fine corsa, oltre a un segnale di zero ripetibile.

Queste funzioni assicurano ai lettori RGH41 una maggiore flessibilità per integrare la varietà di applicazioni in cui viene già utilizzato il sistema RG2: CMM, macchine di layout, macchine per produzione e test di componenti elettronici, motori lineari standard e personalizzati.

Lettori digitali (doppio limite)
RGH41T - risoluzione 10 µm
RGH41D - risoluzione 5 µm
RGH41G - risoluzione 2 µm
RGH41X - risoluzione 1 µm
RGH41N - risoluzione 0,4 µm
RGH41W- risoluzione 0,2 µm
RGH41Y - risoluzione 0,1 µm
RGH41H - risoluzione 50 nm

Lettori analogici
RGH41B - differenziale 1 Vpp (limite singolo)
RGH41A - differenziale 1 Vpp (doppio limite)

- **Sistema ottico aperto senza contatto**
- **Ampie tolleranze di installazione**
- **Funzionamento a una velocità massima di 15 m/s**
- **Uscite digitali e analogiche standard**
- **Risoluzioni da 10 µm a 50 nm**
- **Sensore di zero e doppio sensore di fine corsa integrati**
- **LED di allineamento integrato**
- **Utilizza la scala autoadesiva Renishaw RGS40-S**

Schema generale e dimensioni

Dimensioni e tolleranze in mm

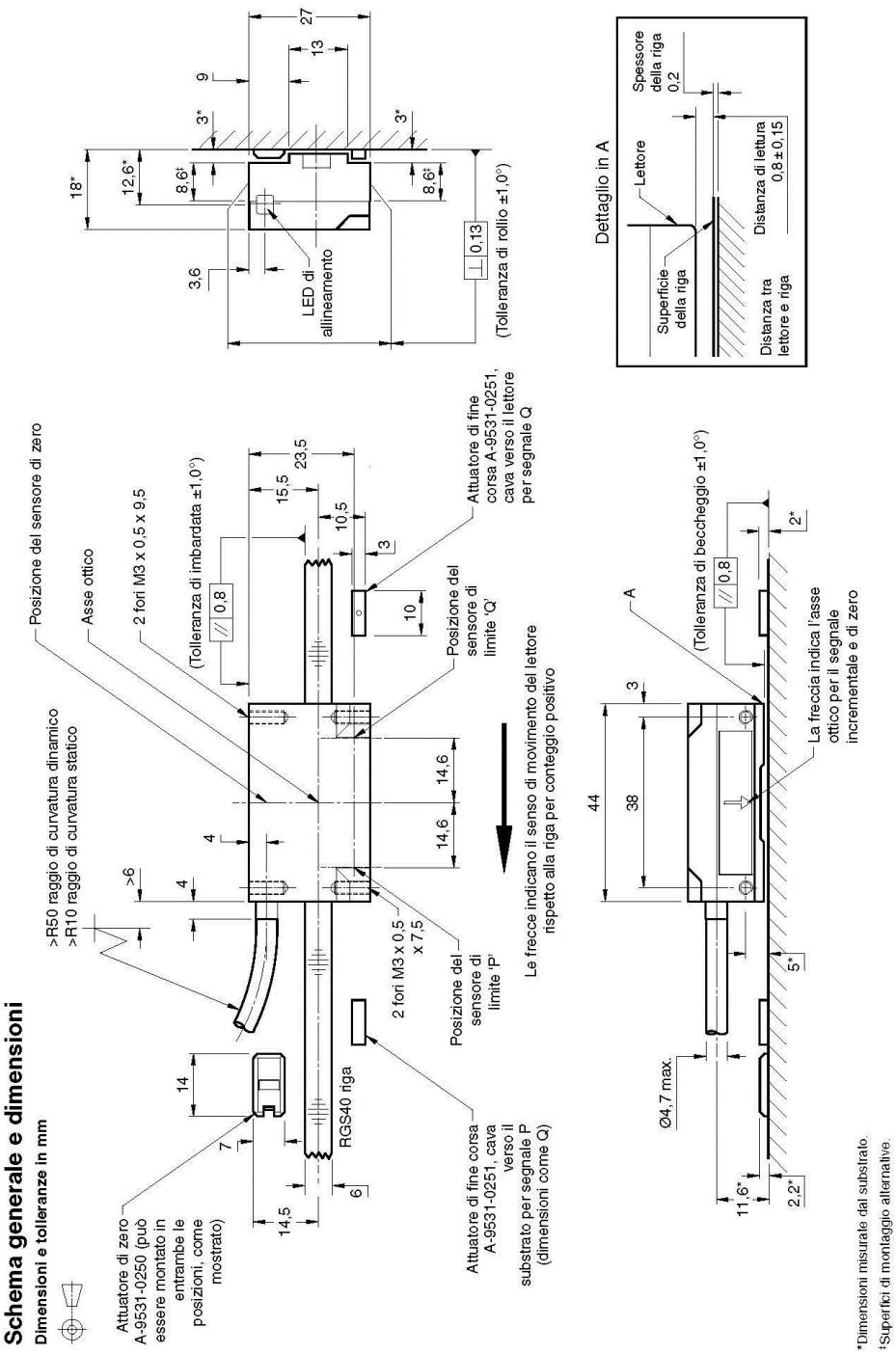

*Dimensioni misurate dal substrato.
‡Superfici di montaggio alternative.

Specifiche dell'uscita

Segnali di uscita digitale - RGH41T, D, G, X, N, W, Y, H

Forma – line driver differenziale EIA RS422A a onda quadra (tranne il limite di fine corsa P, Q, Allarme E e il segnale di setup esterno X)

Incrementali 2 canali A e B in quadratura (sfasati di 90°)

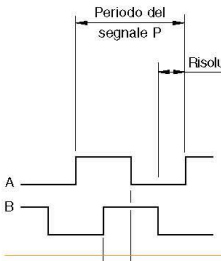

Modell	P (µm)	S (µm)
RGH41T	40	10
RGH41D	20	5
RGH41G	8	2
RGH41X	4	1
RGH41N	1,6	0,4
RGH40W	0,8	0,2
RGH40Y	0,4	0,1
RGH40H	0,2	0,05

Per una maggiore chiarezza, il segnale inverso non è mostrato

Riferimento

Impulso sincronizzato Z, durata in base alla risoluzione S.
Ripetibilità della posizione (unidirezionale) mantenuta entro una temperatura di ± 20 °C al momento della fasatura.
Dispositivo di attuazione A-9531-0250.
Per una maggiore chiarezza, il segnale inverso non è mostrato

Allarme Lettori a limite singolo - linea differenziale
Lettori a limite doppio - linea a terminazione unica

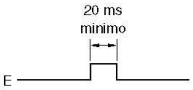

Per una maggiore chiarezza, il segnale inverso non è mostrato E- solo nei lettori a limite doppio (opzione 05/06)

I modelli RGH41T, G, X emettono l'allarme per segnale inferiore al 15%. L'emissione è sotto forma di segnale asincrono E come mostrato a lato (opzioni 03/05) o apertura dei canali in tri-state (opzioni 04-06)

I modelli RGH41N, W, Y, H emettono l'allarme E quando:
- L'ampiezza supera il 150%
- Il lettore supera la velocità massima

Inoltre le uscite entrano in modo tri-state con ampiezza del segnale <15%

Set up esterno

Tra 50% e 70% del segnale, X è un duty cycle, con periodo 20 µm.
Il tempo trascorso a 5V aumenta con il livello del segnale. Con segnale >70% X è pari a 5V nominali.

Uscita collettore aperto di limite

Limite singolo (opzione 03/04)

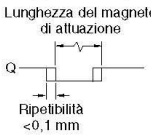

Limite doppio (opzione 05/06)

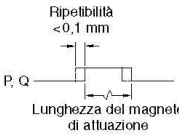

Terminazione

Impulso asincrono P, Q.
Dispositivo di attuazione A-9531-0251, A-9531-2052, A-9531-2054.
*Selezionare R in modo che la corrente massima non superi i 20 mA. In alternativa, è possibile usare un relè o un isolatore ottico adeguato.

Terminazione consigliata per i segnali

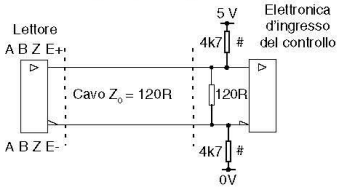

Circuito line receiver standard RS422A.
#Richiesto solo sul canale E per sicurezza contro rottura del cavo e, su RGH41N, W, Y, H, per assicurare che sia riconosciuto l'errore quando i canali si aprono in tri-state

Segnali di uscita analogica - RGH41A, B

Incrementale - Sinusoidi differenziali a 2 canali V_1 e V_2 in quadratura (sfasatie di 90°)

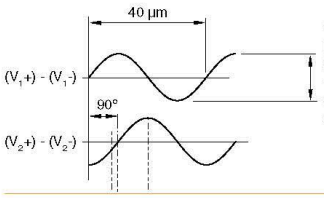

0,6 - 1,2 Vpp con LED verde e terminazione 120R se il segnale viene ricevuto in differenziale.

Riferimento

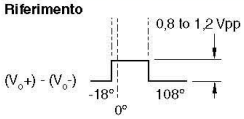

Impulso differenziale V_0 da -18° a 108°.
Durata 126° (elettrici).
Ripetibilità della posizione (unidirezionale) mantenuta entro una temperatura di ± 20 °C al momento della fasatura.
Dispositivo di attuazione A-9531-0250.

Terminazione consigliata per i segnali

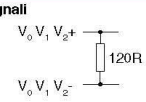

Uscita collettore aperto di limite

RGH41B a limite singolo

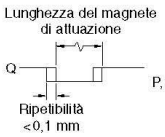

RGH41A a doppio limite

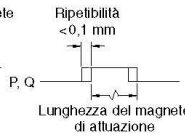

Terminazione

Impulso asincrono P, Q.
Dispositivo di attuazione A-9531-0251, A-9531-2052, A-9531-2054.
*Selezionare R in modo che la corrente massima non superi i 20 mA. In alternativa, è possibile usare un relè o un isolatore ottico adeguato.

External set-up

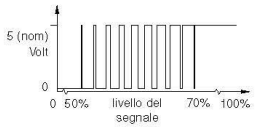

Tra 50% e 70% del segnale, X è un duty cycle, con periodo 20 µm. Il tempo trascorso a 5V aumenta con il livello del segnale. Con segnale >70% X è pari a 5V nominali.

Renishaw S.p.A.,
Via dei Prati 5,
10044 Pianezza,
Torino, Italia

T +39 011 966 10 52
F +39 011 966 40 83
E italy@renishaw.com
www.renishaw.it

RENISHAW
apply innovation™

Specifiche operative ed elettriche

Prestazioni di velocità

Lettori con uscite sotto clock

Le interfacce RGH41N, W, Y, H sono disponibili con diverse frequenze di clock sul segnale d'uscita.

Queste opzioni sono state studiate in modo da evitare che fronti ravvicinati siano ignorati da un'elettronica di ricezione che utilizzi frequenze di clock inferiori. In base alla frequenza di clock scelta, ciascuna opzione ha una diversa velocità massima e una differente frequenza minima di conteggio consigliata.

Lettori digitali

Tipo di testina	Velocità massima (m/s)	Frequenza minima di clock di conteggio consigliata (MHz)
T D G X	15 12 10 6	$\left(\frac{\text{Velocità encoder (m/s)}}{\text{Risoluzione (µm)}}\right)$ Fattore di sicurezza x 4

Opzione N, W, Y, H	N	W	Y	H	Frequenza minima di clock di conteggio consigliata (MHz)
61	3,0	2,5	1,3	0,6	20
62	2,6	1,3	0,7	0,3	10
63	1,3	0,7	0,35	0,15	5

Lettori A/B analogici

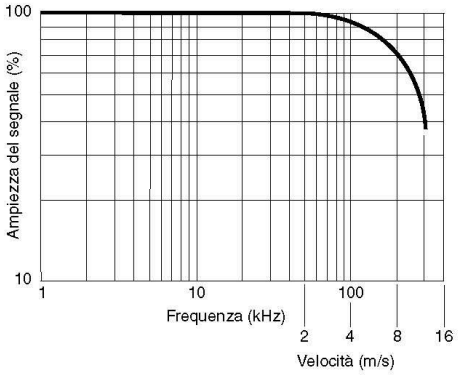

Alimentazione elettrica	5 V± 5%	120 mA (tipica) **NOTA:** Nel caso di uscite digitali i valori di consumo di corrente si riferiscono a lettori senza terminazione. In caso di terminazione a 120 ohm verranno utilizzati ulteriori 25 mA per coppia di canali (ad esempio, A+, A-). I sistemi encoder Renishaw devono essere alimentati con corrente a 5 V CC in modo conforme ai requisiti SELV dello standard EN (IEC) 60950. Ondulazione <200 mV pp con frequenza massima 500 kHz
Temperatura	Immagazzinamento -20 °C to +70 °C	In funzione 0 °C to +55 °C
Umidità	Immagazzinamento: max 95 % di umidità relativa (senza condensa) (IEC 61010-1) In funzione: max 80 % di umidità relativa (senza condensa) (IEC 61010-1)	
Protezione	IP50	
Accelerazione	Funzionamento a 500 m/s² (IEC 60068-2-7)	
Urti (non in funzione)	1000 m/s², 6 m/s, ½ seno (IEC 60068-2-27)	
Vibrazione (in funzione)	100 m/s² max @ 55 a 2000 Hz (IEC 680068-2-6)	
Massa	Lettore 50 g	Cavo 38 g/m
Compatibilità elettromagnetica	BS EN 61326	
Cavo	Cavo a 12 conduttori, doppia schermatura, diametro esterno 4.7 mm Vita a flessione >10 x 10^6 cicli con raggio di piegatura a 50 mm	

Opzioni di connessione	**Codice – tipo di connettore**	**Applicazione**
	D - Connettore di tipo D a 15 pin	RGH41T, D, G, X, N, W, Y, H
	L - Connettore di tipo D a 15 pin	RGH41A, B
	V - Connettore circolare a 12 pin	RGH41B
	W- Connettore circolare a 12 pin senza ghiera	RGH41B
	F - non terminato	Tutti i lettori
	X - Connettore volante a 16 pin	Tutti i lettori

Per indicazioni sui contatti nel mondo visitare il sito principale www.renishaw.it/contattateci

L - 9517 - 9144 - 03

Annex E

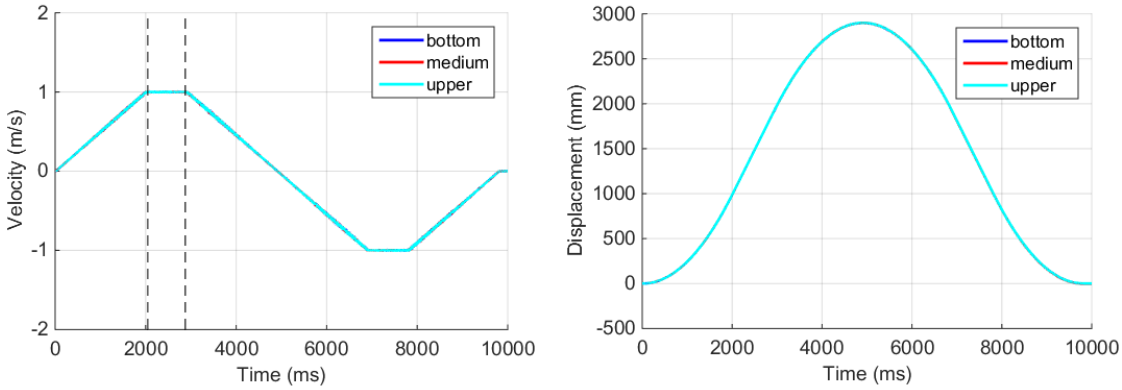

(**a**) Velocity and (**b**) displacement trends acquired by the linear motor encoders during the 1 m/s void test.

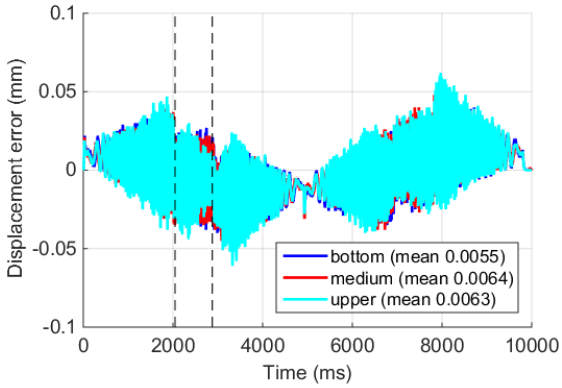

Errors of the three axis in term of displacement (void test 1 m/s).

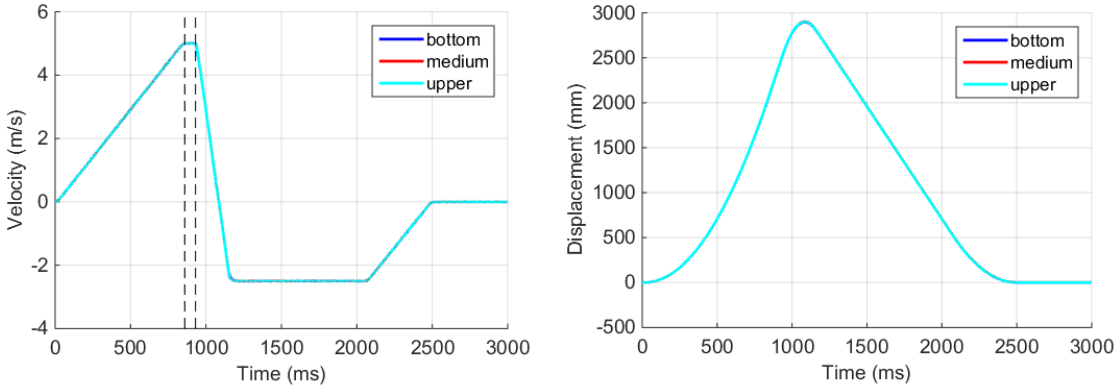

(**a**) Velocity and (**b**) displacement trends acquired by the linear motor encoders during the 5 m/s void test.

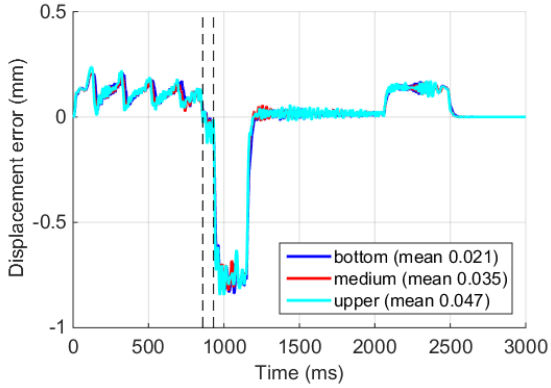

Errors of the three axis in term of displacement (void test 5 m/s).

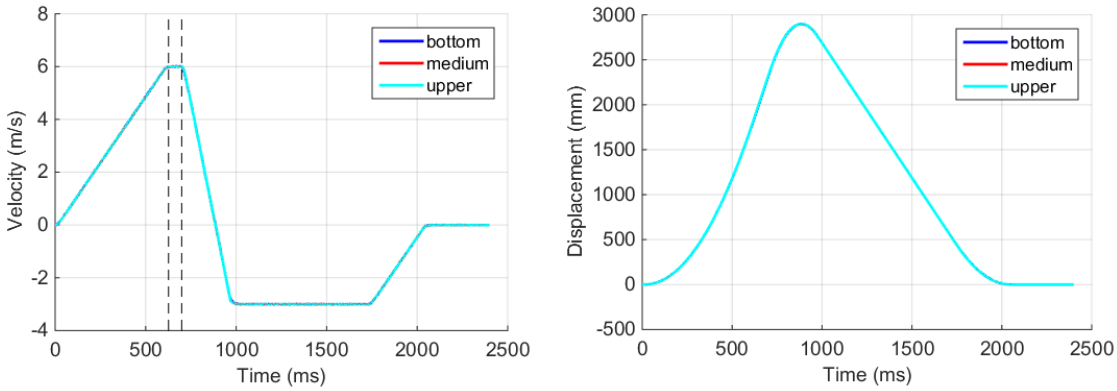

(**a**) Velocity and (**b**) displacement trends acquired by the linear motor encoders during the 6 m/s void test.

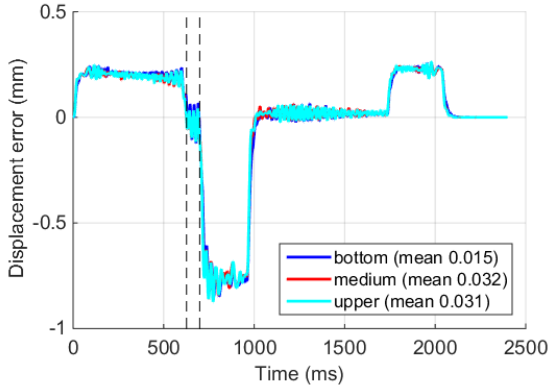

Errors of the three axis in term of displacement (void test 6 m/s).

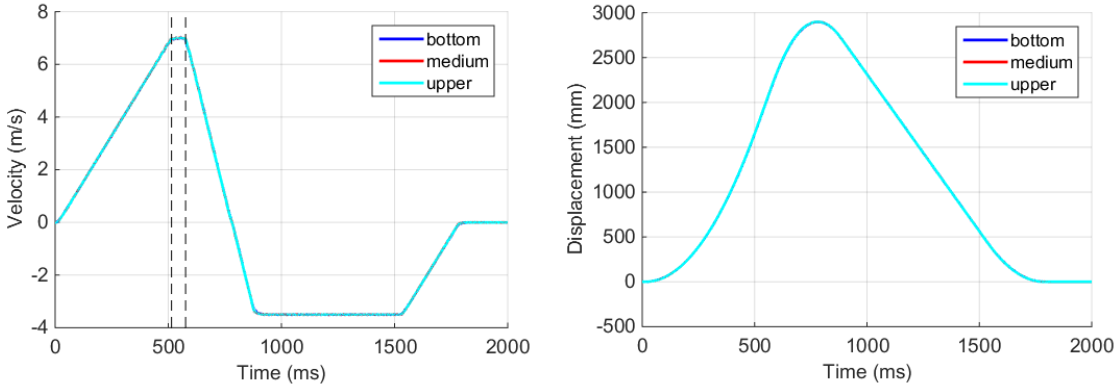

(**a**) Velocity and (**b**) displacement trends acquired by the linear motor encoders during the 7 m/s void test.

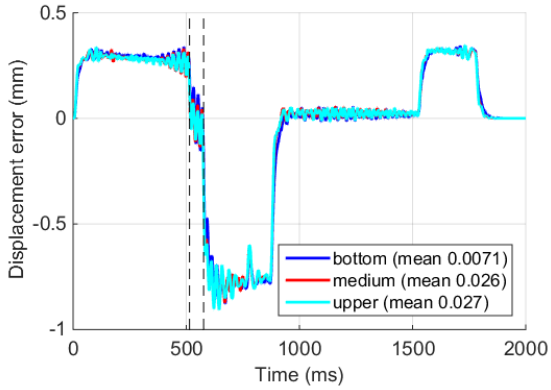

Errors of the three axis in term of displacement (void test 7 m/s).

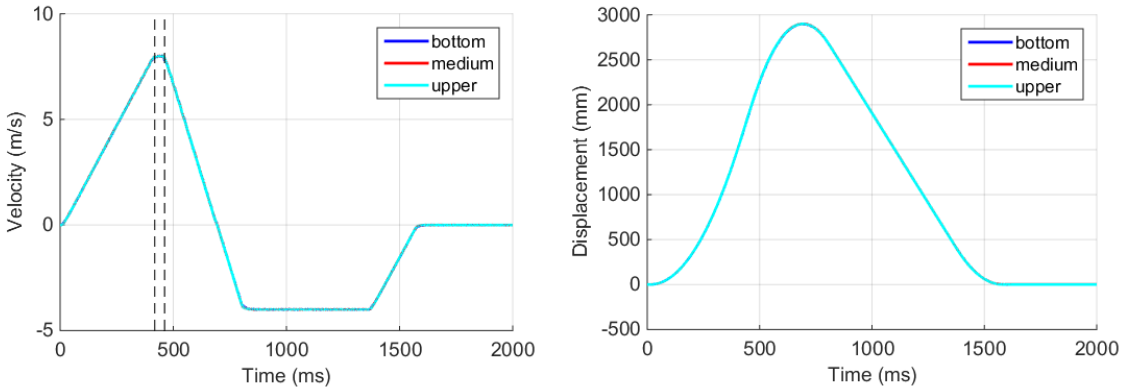

(**a**) Velocity and (**b**) displacement trends acquired by the linear motor encoders during the 8 m/s void test.

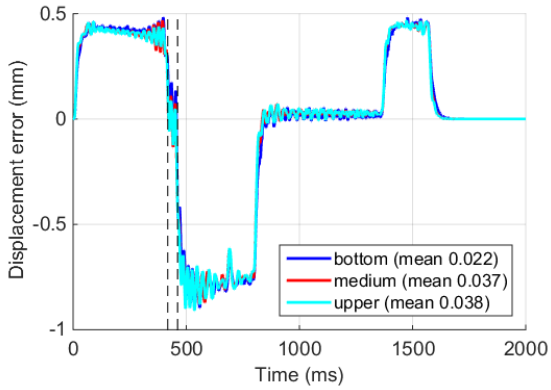

Errors of the three axis in term of displacement (void test 8 m/s).

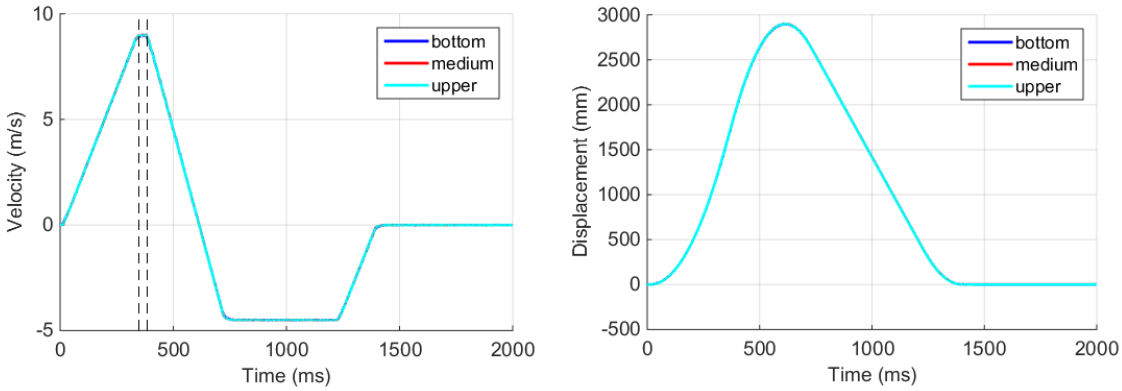

(**a**) Velocity and (**b**) displacement trends acquired by the linear motor encoders during the 9 m/s void test.

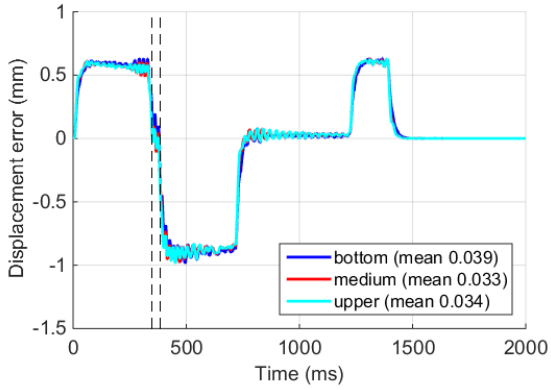

Errors of the three axis in term of displacement (void test 9 m/s).

Annex F (50 kg masses tests)

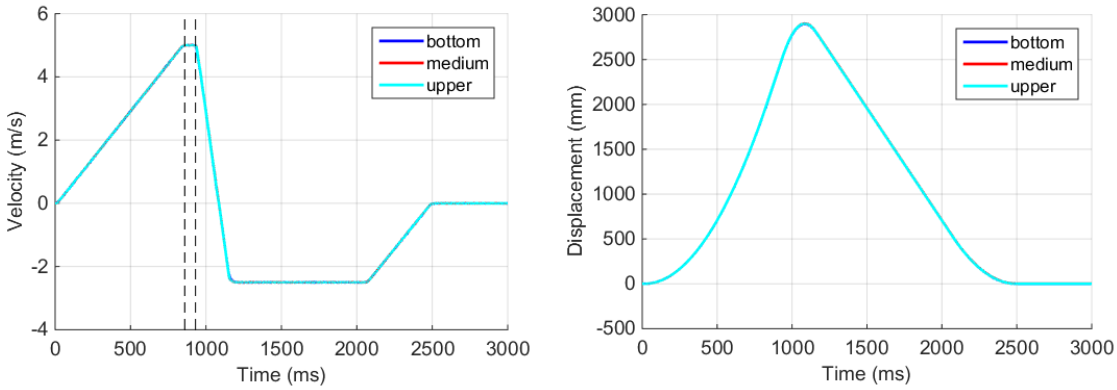

(**a**) Velocity and (**B**) displacement trends acquired by the linear motor encoders during the 5 m/s test with three 50 kg masses.

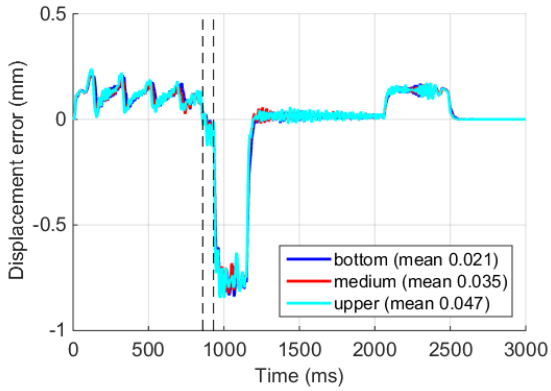

Errors of the three axis in term of displacement (50 kg masses test at 5 m/s).

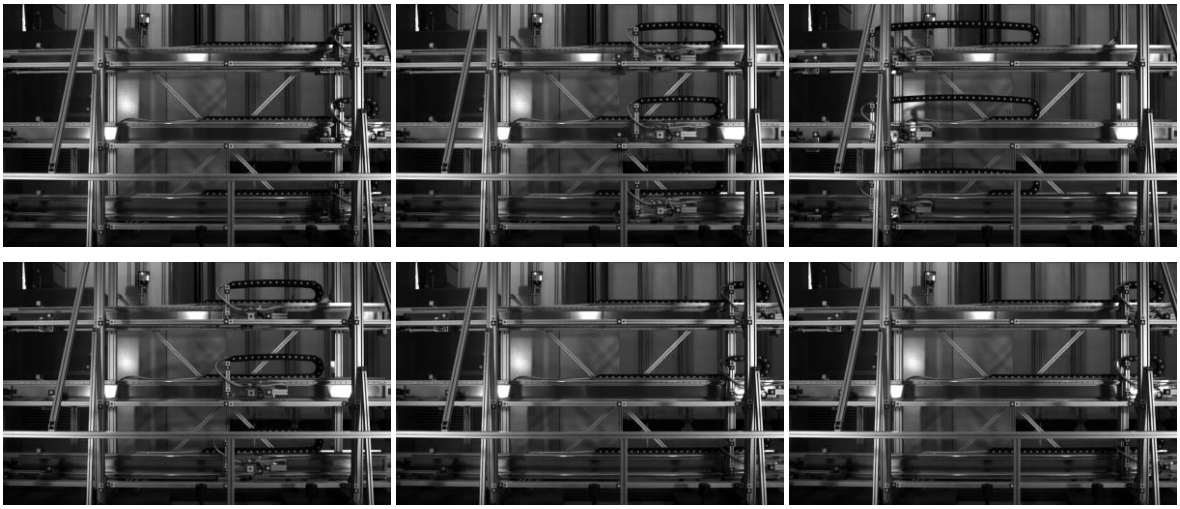

High-speed photo sequence of the 5 m/s test with 50 kg masses

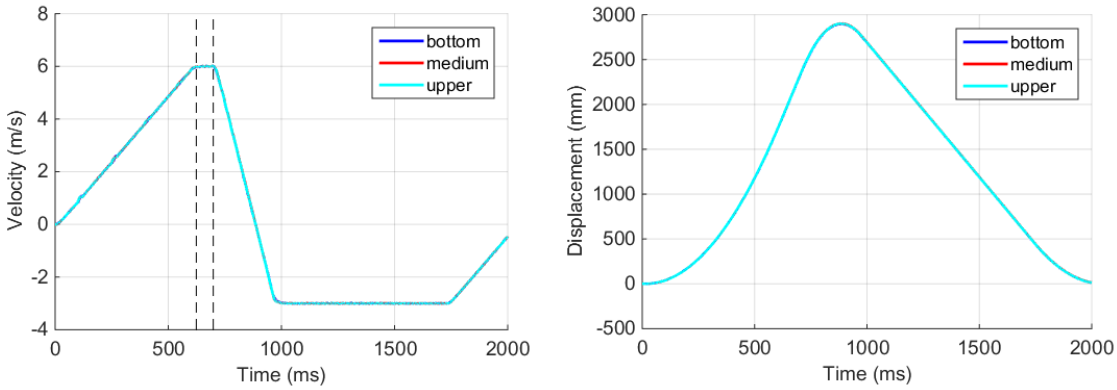

(**a**) Velocity and (**B**) displacement trends acquired by the linear motor encoders during the 6 m/s test with three 50 kg masses.

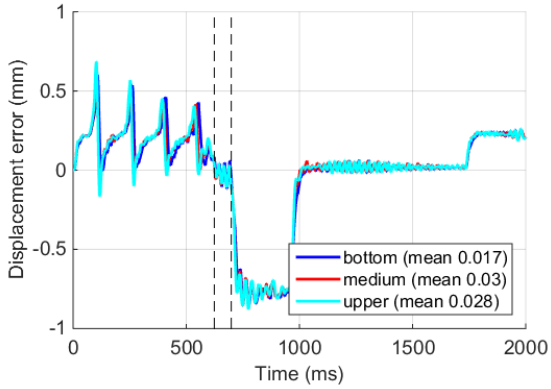

Errors of the three axis in term of displacement (50 kg masses test at 6 m/s).

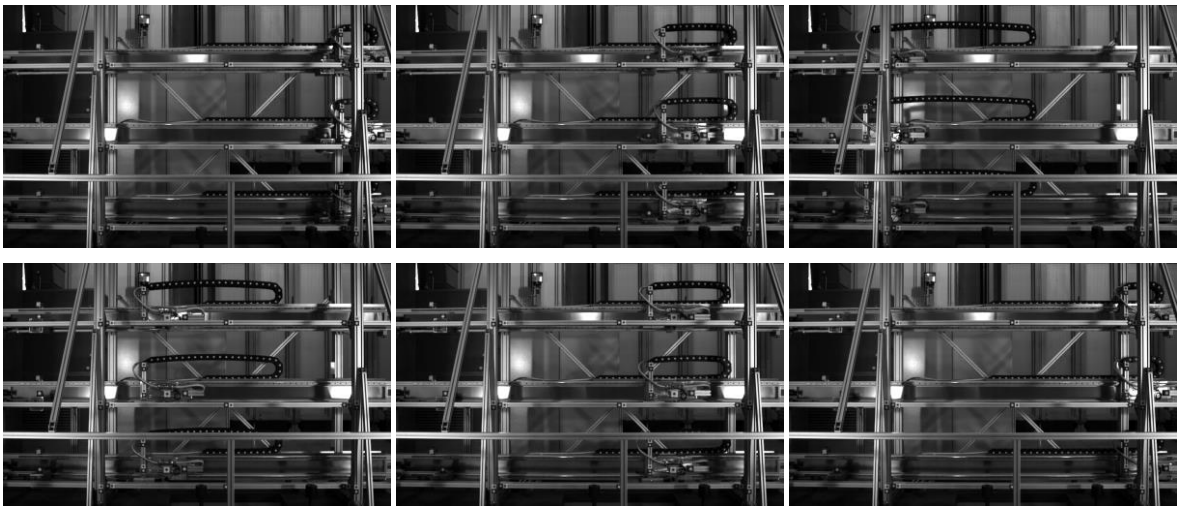

High-speed photo sequence of the 6 m/s test with 50 kg masses

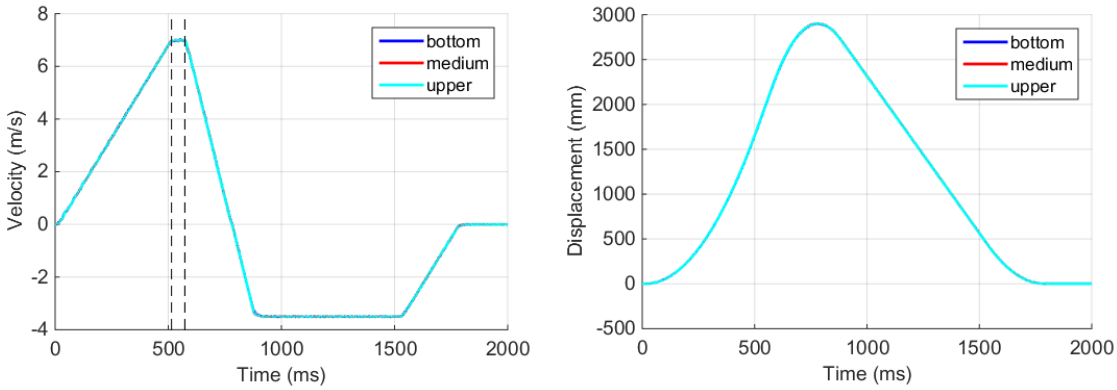

(**a**) Velocity and (**B**) displacement trends acquired by the linear motor encoders during the 7 m/s test with three 50 kg masses.

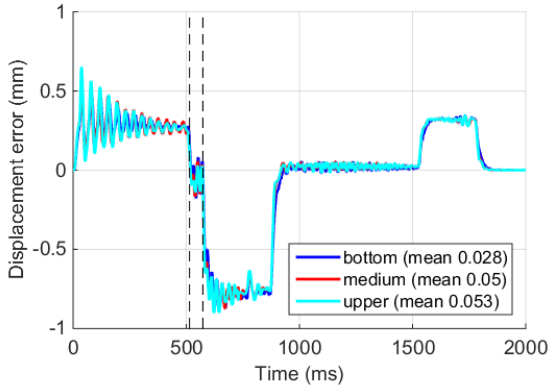

Errors of the three axis in term of displacement (50 kg masses test at 7 m/s).

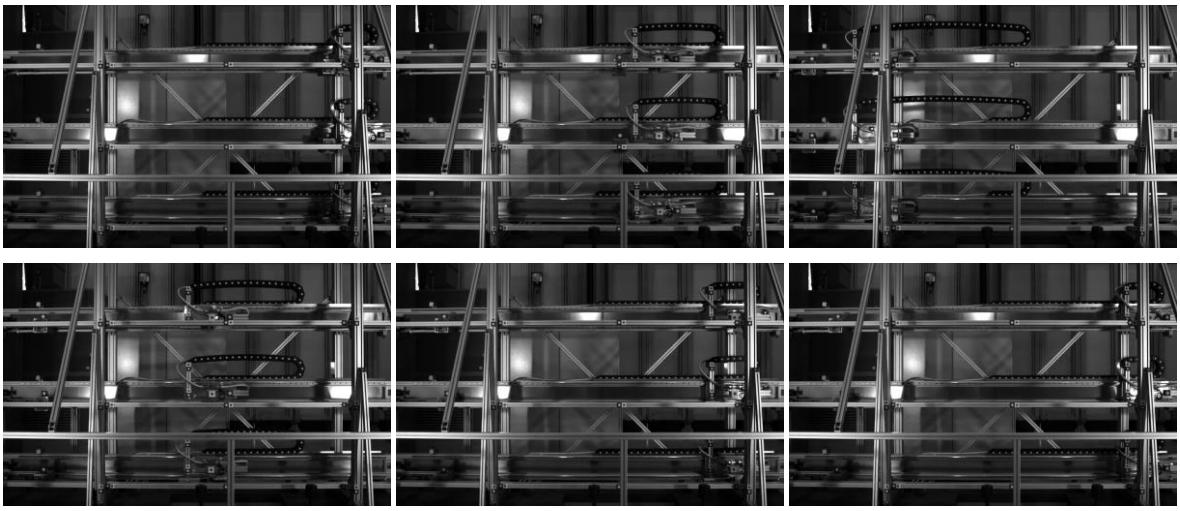

High-speed photo sequence of the 7 m/s test with 50 kg masses

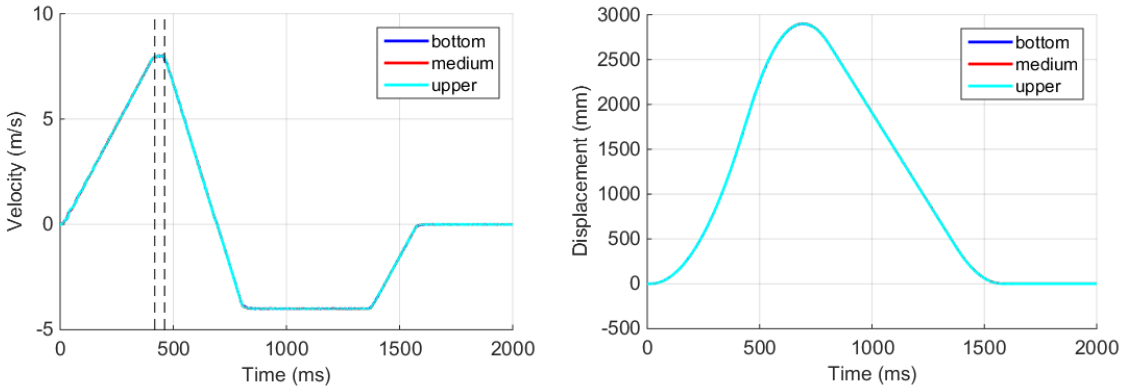

(**a**) Velocity and (**B**) displacement trends acquired by the linear motor encoders during the 8 m/s test with three 50 kg masses.

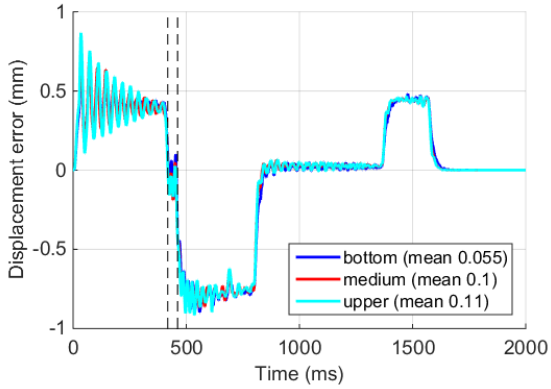

Errors of the three axis in term of displacement (50 kg masses test at 8 m/s).

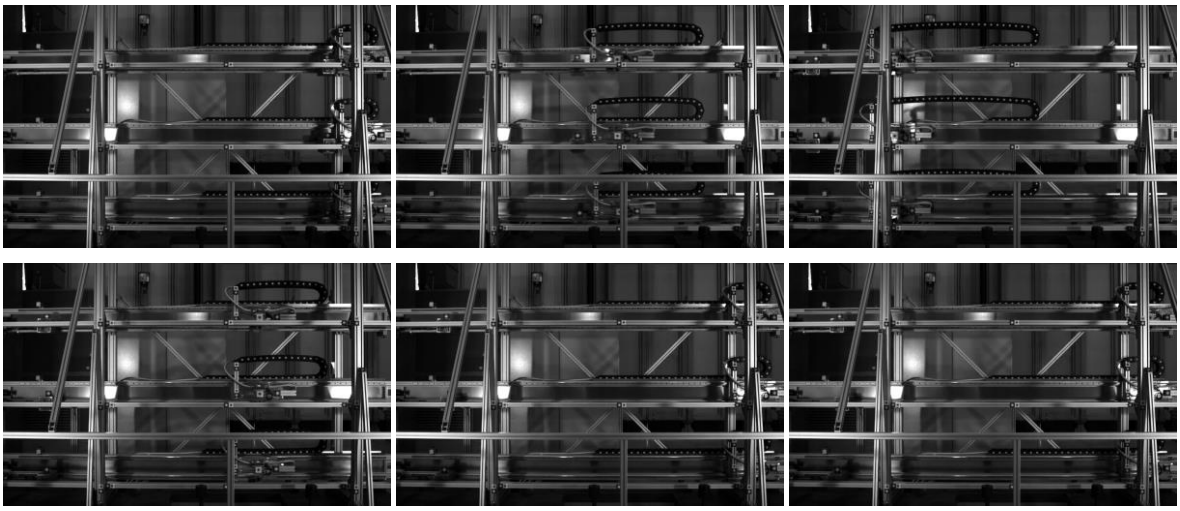

High-speed photo sequence of the 8 m/s test with 50 kg masses

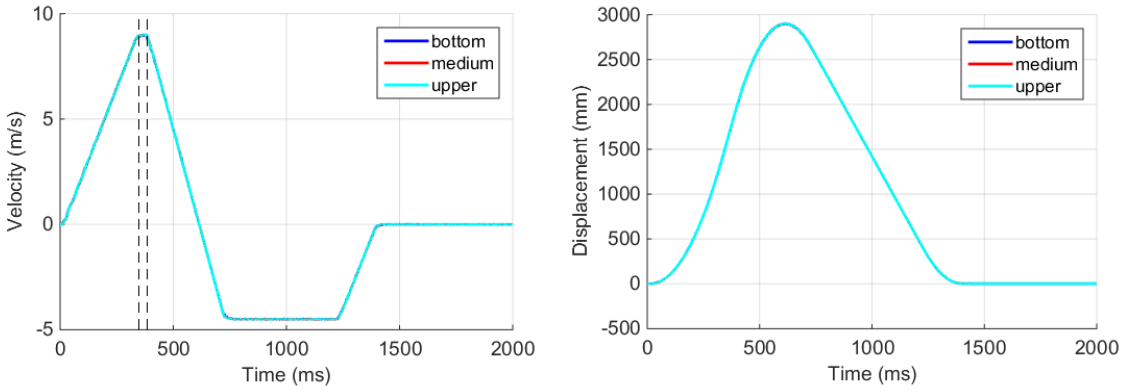

(**a**) Velocity and (**B**) displacement trends acquired by the linear motor encoders during the 9 m/s test with three 50 kg masses.

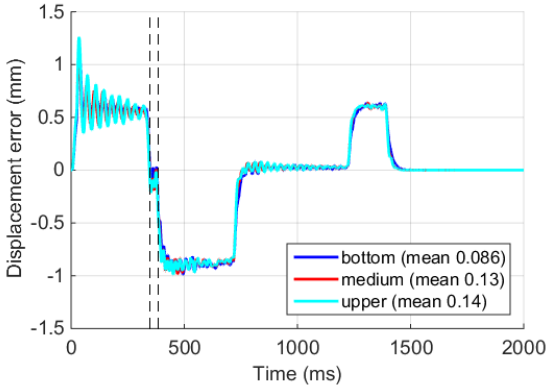

Errors of the three axis in term of displacement (50 kg masses test at 9 m/s).

High-speed photo sequence of the 9 m/s test with 50 kg masses

LB-NA-27652-EN-N

JRC Mission

As the Commission's in-house science service, the Joint Research Centre's mission is to provide EU policies with independent, evidence-based scientific and technical support throughout the whole policy cycle.

Working in close cooperation with policy Directorates-General, the JRC addresses key societal challenges while stimulating innovation through developing new methods, tools and standards, and sharing its know-how with the Member States, the scientific community and international partners.

Serving society
Stimulating innovation
Supporting legislation

Publications Office

doi:10.2788/292788

ISBN 978-92-79-54184-1